Design and Simulator Evaluation of a Structured 2DoF H∞ Loop-Shaping Control Law for a Business Jet

Baptista Marques, J.A.; Stroosma, O.; Theodoulis, S.T.

DOI
10.2514/6.2025-2242

Publication date
2025

Document Version
Final published version

Published in
Proceedings of the AIAA SCITECH 2025 Forum

AIAA SciTech Forum
6-10 January 2025, Orlando, FL
AIAA SCITECH 2025 Forum

10.2514/6.2025-2242

Design and Simulator Evaluation of a Structured 2DoF $\mathcal{H}_\infty$ Loop-Shaping Control Law for a Business Jet

João Marques*, Olaf Stroosma †, and Spilios Theodoulis‡
Delft University of Technology, Kluyverweg 1, 2629 HS Delft, The Netherlands

This paper presents the development process of an aircraft control law. The control law is designed using a two-degree-of-freedom (2DoF) structured $\mathcal{H}_\infty$ loop-shaping approach. This method allows the reuse of controller structures required by certification procedures while directly including handling qualities and robust stability requirements in the optimization process. This strategy is employed to develop a Rate Command and Attitude Hold (RCAH) demand system aimed at satisfying longitudinal handling qualities. First, the stability of the open-loop model and its compliance with the handling qualities guidelines are evaluated. Then, the control law is designed, with a detailed description provided of the design specifications and their formulation in the context of $\mathcal{H}_\infty$ control. Subsequently, the controller parameters are optimized to satisfy the design specifications and a closed-loop analysis is performed. Finally, a simulator flight testing campaign is conducted to experimentally validate the designed control law. It is shown that the aircraft equipped with the RCAH system achieves better handling quality ratings (HQRs) and more favorable pilot feedback, providing a substantial improvement over the bare airframe.

I. Introduction

Flight control laws for transport aircraft traditionally rely on classical control methods, often coupled with straightforward gain scheduling [1]. However, these techniques suffer from performance degradation due to nonlinearities, uncertainties, and failures encountered in reality [2]. One promising way of addressing these problems, while reusing the structures required by the stringent certification processes is through structured $\mathcal{H}_\infty$ control. In addition to certification considerations, compared to previous $\mathcal{H}_\infty$ methods that created full-order controllers, structured $\mathcal{H}_\infty$ control achieves a lower order, minimizing implementation challenges [3], and provides greater transparency in the control design process.

The structured $\mathcal{H}_\infty$ problem can be solved using nonsmooth optimization techniques [4]. In 2014, flight-tested examples showcasing the effectiveness of this method started to appear. More specifically, on space applications [5, 6] and in the aircraft industry [7]. Furthermore, recent advancements in robust control have allowed the tuning of controllers against multiple constraints [8]. A crucial aspect of aircraft flight control systems (FCS) are the handling qualities specifications. To directly incorporate the handling qualities into the $\mathcal{H}_\infty$ problem, the robust two-degree-of-freedom (2DoF) design approach was proposed [9]. Combining the 2DoF architecture with the multi-objective structured controller design approach is thus a recent possibility that is expected to generate promising results.

Therefore, the contribution of this paper is to extensively present the development process of a structured 2DoF $\mathcal{H}_\infty$ control law from the design process to the flight test validation on a simulator. The selected demand system is a Rate Command and Attitude Hold (RCAH) focused on the pitch axis. Moreover, a particular type of $\mathcal{H}_\infty$ strategy, namely $\mathcal{H}_\infty$ loop-shaping [10], was preferred. This strategy has the added benefits of providing guaranteed phase and gain margins [11] and clear management of conflicting specifications [12].

The primary objective of this research is to determine whether the developed control law can satisfy longitudinal handling quality requirements in considerably different flight conditions using only one set of controller parameters. Additionally, the study aims to assess if adding the RCAH system improves handling qualities when compared to the bare-airframe aircraft. Success in this would demonstrate remarkable robust performance, validating the benefits of the proposed control approach.

For this work, a CS-25 certifed Cessna Citation II was chosen as testbench. This aircraft is mainly used for research and has experienced the flight testing of several modern control strategies such as Incremental Nonlinear Control (INDI) [13, 14], Incremental Backstepping Control [15], Reinforcement Learning (RL) [16] and Linear Parameter

*MSc. Student, Control & Simulation Section, Faculty of Aerospace Engineering, Student AIAA Member.
†Senior Researcher, Control & Simulation Section, Faculty of Aerospace Engineering, Senior AIAA Member.
‡Associate Professor, Control & Simulation Section, Faculty of Aerospace Engineering, Associate Fellow AIAA Member.

Varying (LPV) Control [1]. Most recently, a new approach using Linear Quadratic (LQ) Control has also been explored, although it has not yet been flight-tested [17]. A nonlinear model of the aircraft, essential for designing the model-based controller, is also available.

Extensive research has also been conducted on other Cessna Citation models. For the Cessna Citation X, a Linear Quadratic Regulator (LQR) method combined with a differential evolution algorithm to optimize weighting matrices was used to satisfy certain handling quality requirements [18]. In another instance, an $\mathcal{H}_\infty$ mixed-sensitivity solution once again combined with meta-heuristics was developed to achieve a control system capable of satisfying specifications despite uncertainties [19]. Lastly, for the Cessna Citation CJ1, a piloted simulation assessment of handling qualities was performed to test a control law designed with a handling qualities optimization-based approach [20].

The final control law produced in this work will be evaluated through a piloted assessment of the longitudinal handling qualities. The flight testing campaign is to be carried out in the SIMONA Research Simulator (SRS) at TU Delft [21]. This simulator is equipped with a six-degree-of-freedom motion system and is currently also being used to evaluate the handling qualities of novel aircraft concepts such as the Flying-V [22, 23].

The outline of the article is as follows: Section II contextualizes the research and presents the relevant theoretical background. Section III formulates and analyses the open-loop model. Section IV describes in detail the design process of the control law. Section V performs a theoretical analysis of the closed-loop system. Section VI presents and discusses the results of the flight testing campaign that experimentally evaluated the handling qualities of the aircraft. Lastly, Section VII gives some final remarks about the conducted research.

II. Background

A. PH-LAB Cessna Citation and SIMONA Simulator

The Cessna Citation II is a research aircraft jointly operated by Delft University of Technology and the Netherlands National Aerospace Laboratory (NLR). Registered as PH-LAB, this twin-jet business aircraft was crafted by Cessna and features two Pratt & Whitney JT15D-4 turbofan engines, each providing a static thrust of 11.12 kN. The aircraft is equipped with numerous facilities to accommodate flight testing including a Fly-By-Wire (FBW) system, Flight Test Instrumentation System (FTIS), and various sensors [13].

Nevertheless, the use of real aircraft to perform flight tests is expensive and is usually used as the final step of the FCS validation process. Instead, the designed control law will be validated using a high-fidelity model of the PH-LAB Cessna Citation aircraft. This aircraft model is a nonlinear model of the Cessna Citation I. The model was developed in the Delft University Aircraft Simulation Model and Analysis Tool (DASMAT) [24]. The Cessna Citation II is a more recent iteration of the Cessna Citation I with increased seating capacity and improved flight performance. The Citation II features more powerful engines, a longer fuselage, and longer wings. Despite these differences, the Citation I DASMAT model fits reasonably well with the flight data of the Citation II [25]. The model will be implemented in the SIMONA Research Simulator to validate the control law through piloted simulator tests.

Fig. 1 PH-LAB Cessna Citation II.

Fig. 2 SIMONA Research Simulator.

B. $\mathcal{H}_\infty$ Loop-Shaping Method

1. Coprime Factor Uncertainty

The coprime factorization form is a representation of system uncertainty that is essential for the powerful control strategy of $\mathcal{H}_\infty$ loop-shaping. Given a system G, the left coprime factorization is

$$G(s) = M_l^{-1}(s)N_l(s) \tag{1}$$

where $M_l(s)$ and $N_l(s)$ are stable coprime functions. Stability dictates that $N_l(s)$ must encompass all the right-half plane (RHP) zeros of $G(s)$, while $M_l(s)$ should include as RHP-zeros all the RHP-poles that $G(s)$ possesses.

Coprimeness, on the other hand, requires that there are no common RHP-zeros shared between $N_l(s)$ and $M_l(s)$. This condition ensures the absence of pole-zero cancellations when forming $M_l^{-1}N_l$. In mathematical terms, coprimeness signifies the existence of stable transfer functions/matrices, denoted as $U_l(s)$ and $V_l(s)$, such that the following equation holds:

$$N_l U_l + M_l V_l = I \tag{2}$$

Now introduce the operator M^* defined as $M^*(s) = M^T(-s)$. Then $G(s) = M_l(s)^{-1}N_l(s)$ is called a normalized left coprime factorization if

$$M_l M_l^* + N_l N_l^* = I \tag{3}$$

An uncertain plant model G_p can then be written as

$$G_p = \{(M_l + \Delta_M)^{-1}(N_l + \Delta_N) : \left\| \begin{bmatrix} \Delta_N & \Delta_M \end{bmatrix} \right\|_\infty < \epsilon\} \tag{4}$$

where Δ_M and Δ_N are stable unknown transfer function matrices that represent the uncertainty in the nominal plant model G, as seen in Figure 3.

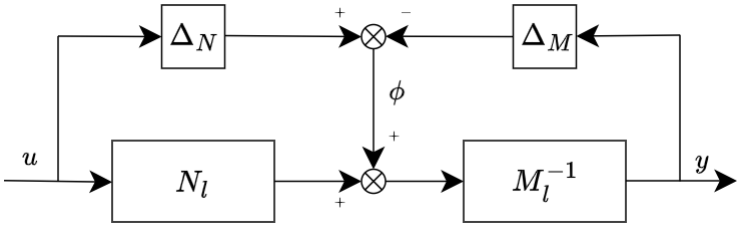

Fig. 3 Coprime factor uncertainty representation of an uncertain plant model G_p.

2. Loop-Shaping

The first step of the $\mathcal{H}_\infty$ loop-shaping design procedure is to use a pre-compensator W_1 and/or post-compensator W_2 to shape the singular values of the nominal plant G. All together, W_1, G, and W_2 form the so-called shaped plant G_s defined by

$$G_s = W_2 G W_1 \tag{5}$$

Tuning W_1 and W_2 is not straightforward. Nevertheless, the following general guidelines can usually be followed [12]:

- High gain at low frequencies;
- Low gain at high frequencies.

High gain at low frequencies guarantees disturbance rejection and good reference tracking properties. Low gain at high frequencies ensures noise attenuation, control signal reduction, and robust stability against unstructured uncertainty. Figure 4 illustrates the guidelines using the singular values of G_s. Additionally, W_1 and W_2 may sometimes contain gains to scale the outputs and make a distinction between their importance [26]. Lastly, it should be checked that the compensators are not canceling any poles or zeros of G. In contrast to classical loop-shaping, the approach adopted in $\mathcal{H}_\infty$ loop-shaping is to shape the open-loop gain without consideration for closed-loop stability. Addressing closed-loop stability will be treated in the next step of the design procedure.

3. Robust Stabilization Against NCF Uncertainty

The achieved shaped plant G_s considered only gain and ignored phase requirements which means G_s is not necessarily closed-loop stable. Therefore, the goal at this stage is to stabilize all perturbed plants G_p defined in Eq. (4), assuming $G_s = M_l^{-1} N_l$. The maximum stability margin $\epsilon_{\max}$ obtainable by closing the loop as shown in Figure 5a, is given by the following $\mathcal{H}_\infty$ problem:

$$\epsilon_{\max}^{-1} = \inf_{K_\infty \text{stabilizing}} \left\| \begin{bmatrix} I \\ K_\infty \end{bmatrix} (I - G_s K_\infty)^{-1} \tilde{M}_s^{-1} \right\|_\infty \tag{6}$$

The above equation should be read as finding the stabilizing controller K that minimizes the $\mathcal{H}_\infty$ norm of the specified transfer matrix. If $\epsilon_{\max} \ll 1$, then one should go back to the first step and adjust W_1 and W_2. If this is not the case, then a stabilizing K_∞ should be selected and the final controller can be obtained using

$$K = W_1 K_\infty W_2 \tag{7}$$

as demonstrated in Figure 5b.

The $\mathcal{H}_\infty$ loop-shaping design procedure is an iterative process where adjustments on the loop-shape and posterior evaluation of achievable robust stability are done several times. To avoid a constant back and forth, some additional aspects might be taken into consideration. Usually, opting for diagonal weights W_1 and W_2 and avoiding high roll-off rates (i.e. maintaining distance between ω_l and ω_h) reduces the amount of iteration needed.

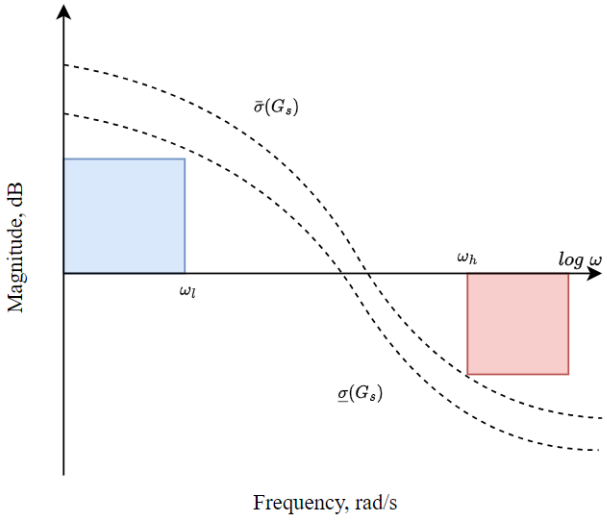

Fig. 4 $\mathcal{H}_\infty$ loop-shaping general guidelines.

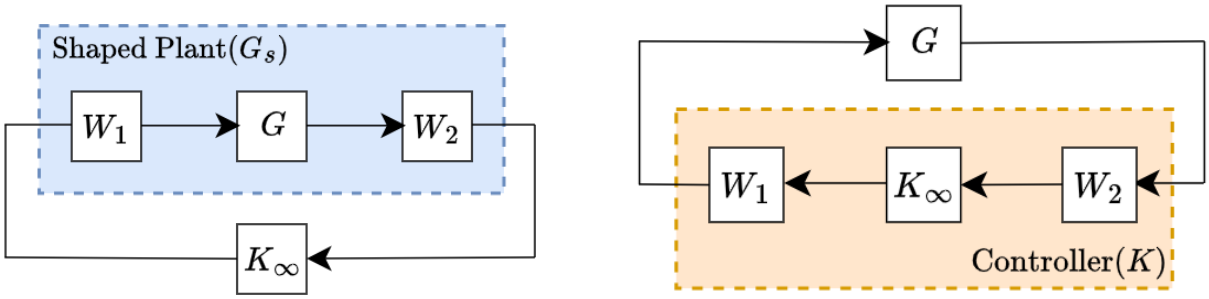

(a) Robustification against NCF uncertainty problem layout. **(b) Final controller.**

Fig. 5 $\mathcal{H}_\infty$ loop-shaping design procedure.

C. Selection of Handling Quality Requirements

Handling qualities are succinctly defined as "those qualities or characteristics of an aircraft that govern the ease and precision with which a pilot is able to perform the tasks required in support of an aircraft role" [27]. Despite extensive research over the years, the assessment of piloted aircraft's handling qualities continues to heavily rely on the subjective judgments of experienced test pilots. Nevertheless, there are quantitative measures that are highly correlated with pilot satisfaction. These are commonly known as theoretical handling qualities. These requirements can be found in the US Department of Defence military handbook *MIL-STD-1797A* [28] or in the works of Gibson [29] and will be used as design specifications. The relevant longitudinal handling quality criteria will be introduced.

1. Low Order Equivalent System (LOES)

The high-order pitch rate frequency response of a classical aircraft to an elevator input can be approximated by a *low order equivalent system* (LOES) of the following type:

$$\frac{q(s)}{\delta_e(s)} = \frac{K_q(s + \frac{1}{T_{\theta 2}})e^{-\tau_e s}}{s^2 + 2\xi\omega_n s + \omega_n^2} \tag{8}$$

The parameter $e^{-\tau_e s}$ is the system phase delay and is intended to approximate the accumulated phase lag arising from all of the additional dynamics in the high-order system transfer equation. Using fitting processes, it is possible to obtain values for the variables shown in Eq. (8). Table 1 presents the limits for the equivalent time delay τ_e. Limits on the other variables of the LOES will be taken into consideration by subsequent requirements.

Table 1 Maximum allowable value of equivalent time delay τ_e for each handling quality level [28].

Level	τ_e, s
Level 1	0.10
Level 2	0.20
Level 3	0.25

2. Control Anticipation Parameter (CAP)

The control anticipation parameter (CAP) criterion proposes that the pilot's ability to predict a flight path response is related to the ratio of the initial pitching acceleration to the steady state load factor following a step control input [29]. The CAP is perhaps the most used handling quality requirement when designing and validating pitch axis controllers [20, 30, 31]. After obtaining a LOES of the short-period mode of the aircraft, the CAP can be obtained through:

$$\text{CAP} = \frac{\dot{q}(0)}{n_z(\infty)} \approx \frac{g\omega_n^2 T_{\theta 2}}{V_{TAS}} \tag{9}$$

The used limits for the values of the CAP and the short-period damping ratio ξ are as defined in the *MIL-STD-1797A* [28].

3. Gibson Dropback Criterion

The Gibson dropback criterion measures the quality of the attitude response. This specific criterion defines limiting values on pitch rate overshoot ratio q_m/q_s and on the ratio of attitude dropback DB/q_s (or overshoot, depending on the direction of the transition when the step input is removed) to steady state pitch rate. These bounds can be found in Gibson's thesis [29].

III. Formulation and Analysis of the Linear Model of the PH-LAB Cessna Citation

A. Flight and Trim Envelopes

The conventional definition of the flight envelope refers to a region of airspeed and altitude where an aircraft is required to operate or a constrained area in the velocity versus load factor graph. To determine an aircraft's flight envelope, several physical phenomena and limiting effects must be considered. These include aerodynamic, structural, and performance limits, controllability requirements, stability margins, and aircraft degradation effects. The *EASA.IM.A.207: Cessna 500, 550, S550, 560 and 560XL* [32] document includes information on the technical characteristics and operational limitations of the Cessna Citation II. Using those values, the flight envelope of Figure 6 was generated.

Once the flight envelope is established, the concept of steady-state flight becomes critical. Steady-state flight provides an initial condition for flight simulation and a flight condition where the aircraft dynamics can be linearized [33]. The process of finding the steady-state values of the control and state vectors is designated as "trimming". In the case of this research, the aircraft was trimmed for straight and leveled flight. Figure 6 shows a set of obtained trim points for a mass of m = 5000 kg, landing gear up, and no flap deflection.

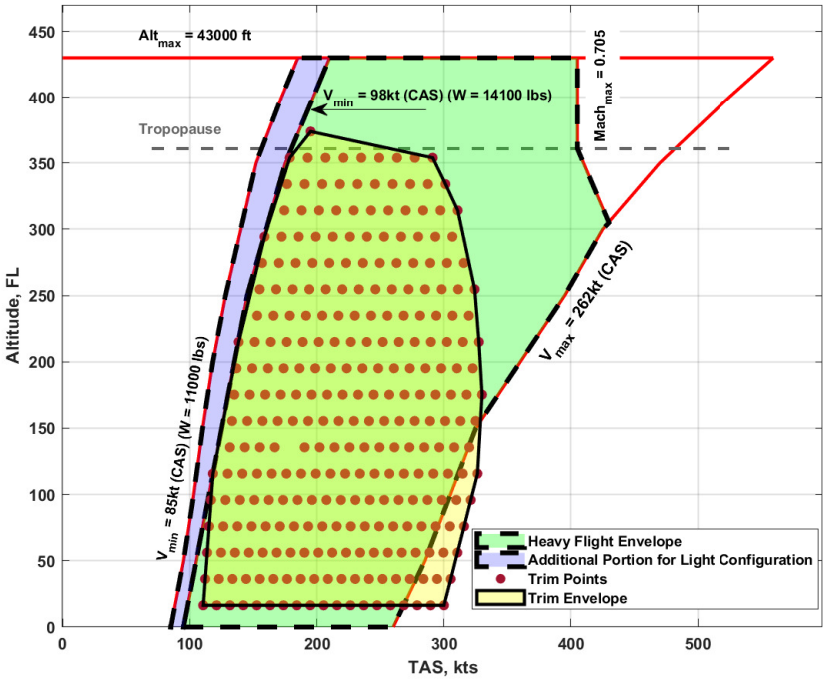

Fig. 6 Flight and trim envelopes.

B. Variable Definitions and State Space Model

The specifications, design procedure, and analysis tools for evaluating the aircraft rely on a linear model. Linear models assume small deviations from an equilibrium point, allowing for a linearized version of the aircraft's motion equations through a Taylor series expansion, retaining only the first-order terms. These linear models are only valid in conditions near the equilibrium point, making any analysis dependent on the creation of several linear models across the entire flight envelope.

A set of linear models of the aircraft was obtained by linearizing the model around each trim point. In total, 280 linear state-space models were obtained. The linear time-invariant (LTI) model describing the longitudinal dynamics of the Cessna Citation consists of four states and one control input and is of the form:

$$\dot{x}(t) = Ax(t) + Bu(t), \quad A \in R^{4\times4}, \quad B \in R^{4\times1} \tag{10}$$

where:

$$x = \begin{bmatrix} q & \alpha & V_{TAS} & \theta \end{bmatrix}^T \tag{11}$$

$$u = \delta_e \tag{12}$$

Another way of representing LTI systems is through transfer functions H (or transfer matrices in the MIMO case). These can be obtained from the state space using the Laplace operator s as follows:

$$H(s) = C(sI - A)^{-1}B + D \tag{13}$$

where matrices C and D define the system's outputs as a linear combination of the states and inputs, respectively.

C. Longitudinal Stability Analysis

The condition for total stability (meaning, both static and dynamic stability) in the Laplace domain is to have all the eigenvalues (λ) of matrix A in the left-half plane (LHP) of the complex plane, such that:

$$\Re(\lambda) < 0 \tag{14}$$

Figure 7 shows the pole-zero map of the transfer function from the input δ_e to the output q. The poles correspond to the eigenvalues of matrix A. As can be seen, all the eigenvalues have a negative real part, and hence the aircraft is longitudinally stable for the entirety of the trim envelope. This result hints at the fact that the RCAH system probably will not need α feedback to provide more stability. The difference between the location of the characteristic poles and zeros of the two longitudinal modes (i.e. short-period and phugoid mode) is clear in the figure. It can be concluded that the two modes are well-separated. The phugoid mode which is a slower and less-damped mode has its poles and zeros more distinctly shown in Figure 7b which corresponds to the zone inside the red rectangle in Figure 7a. All the poles and zeros outside this zone are characteristic of the short-period mode.

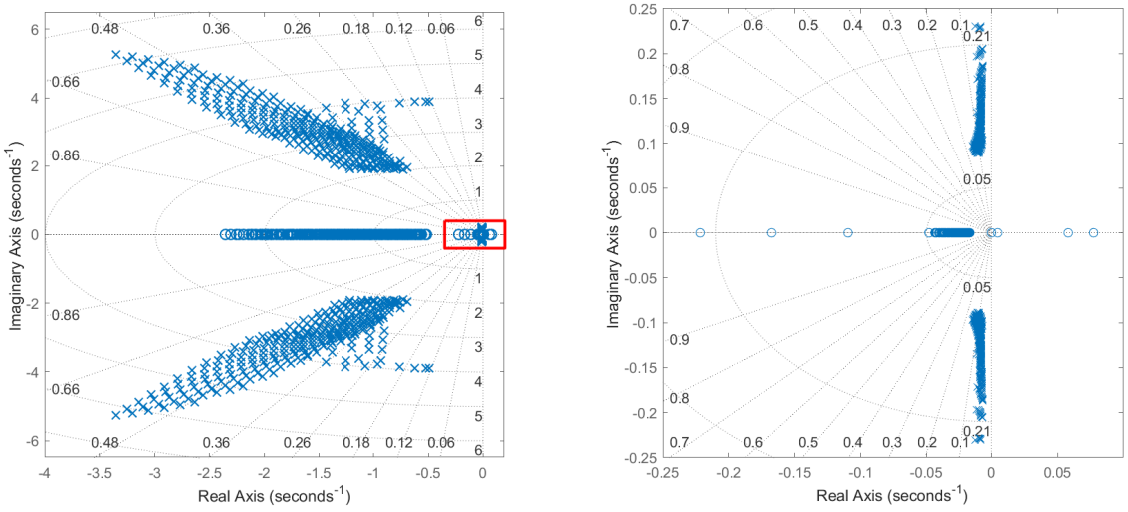

(a) Zoom out. **(b) Zoom in on the phugoid characteristic poles and zeros.**

Fig. 7 Open-loop system pole-zero map from input δ_e to output q.

D. Reduced Order Model

So far, one element has been left out of the conversation: the human pilot. If the aircraft is to be flown by a human pilot, as is the case of the PH-LAB Cessna Citation, the relative importance of the eigenmodes changes according to the characteristics of the pilot. The short-period gains a prominent role in this case since it possesses a natural frequency closer to that of the pilots. Conversely, since the phugoid mode is such a slow mode its influence on the successful accomplishment of a task is much lesser. Therefore, it would be convenient to obtain a reduced-order model in which the phugoid is suppressed or omitted. Obtaining such a reduced-order model has been a widely explored concept in the field of flight dynamics and can be obtained through the so-called short-period approximation (see e.g. [33]). The reduced linear state space model has the following form:

$$\dot{x}(t) = A_{\text{red}}x(t) + B_{\text{red}}u(t), \quad A_{\text{red}} \in R^{2\times 2}, \quad B_{\text{red}} \in R^{2\times 1} \tag{15}$$

where:

$$x = \begin{bmatrix} q & \alpha \end{bmatrix}^T \tag{16}$$

$$u = \delta_e \tag{17}$$

The full and reduced LTI models of the flight condition shown in Table 2 were thoroughly analyzed.

Table 2 Flight condition data.

Height	TAS	Mach
3526 m	120 m/s	0.3684

Figure 8 compares the full-order and short-period approximation pitch rate transfer functions. The magnitude plot indicates a significant peak in the response at a frequency nearly matching the natural frequency of the lightly damped phugoid mode. Additionally, there is a smaller peak corresponding to the more heavily damped short-period mode. The figure proves that the short-period approximation is a good approximation to the pitch-rate transfer function at frequencies above $\omega_n = 0.3$ rad/s.

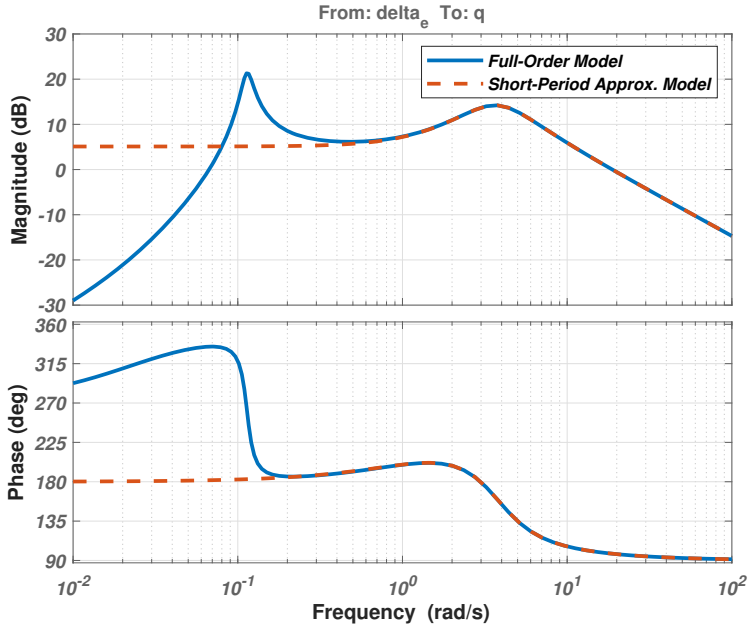

Fig. 8 Bode plot comparing the full-order model and short-period approximation pitch rate transfer functions.

E. Comparison with the Handling Quality Requirements

With stability ensured, the next step is to analyze the theoretical handling qualities of the open-loop aircraft, also known as bare-airframe aircraft. To be even clearer, the bare airframe refers to the aircraft without any control or stability augmentation system. In this configuration, the pilot directly controls the actuators using the available control inceptors (e.g., sidestick, throttle, control column). Figure 9 portrays the bare airframe layout. The depicted aircraft model is the short-period approximation model. The actuator was modeled as follows:

$$\frac{\delta_e}{\delta_{e_{com}}} = \frac{1}{0.0769s + 1} \tag{18}$$

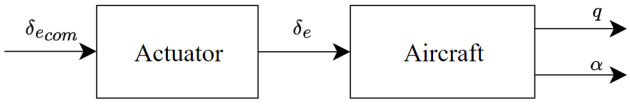

Fig. 9 Bare airframe layout.

Figure 10 shows how the Gibson dropback criterion satisfaction is distributed across the trim envelope for the bare-airframe aircraft. It can be seen that for the majority of the envelope, this handling quality requirement is not satisfied. Only for some points at low altitude and high speed is the response acceptable. The main issue seems to be an excessive dropback. It is then predicted that the pilots will experience a certain degree of bobbling when performing attitude control tasks with the bare-airframe aircraft. Figure 11 gives the values of the CAP and the short period damping ratio for every flight point and illustrates how the CAP criterion is being satisfied across the trim envelope. It can be concluded that the CAP criterion is satisfied for the great majority of tested flight points. The exception are some points at low speeds close to the stalling speed of the aircraft. Hence, for the level 1 points, it is anticipated that the pilot will be able to predict the flight path response of the bare-airframe aircraft. Finally, Figure 12 presents the values of the equivalent time delay for the total 280 flight points. This last criterion is satisfied for every studied flight point.

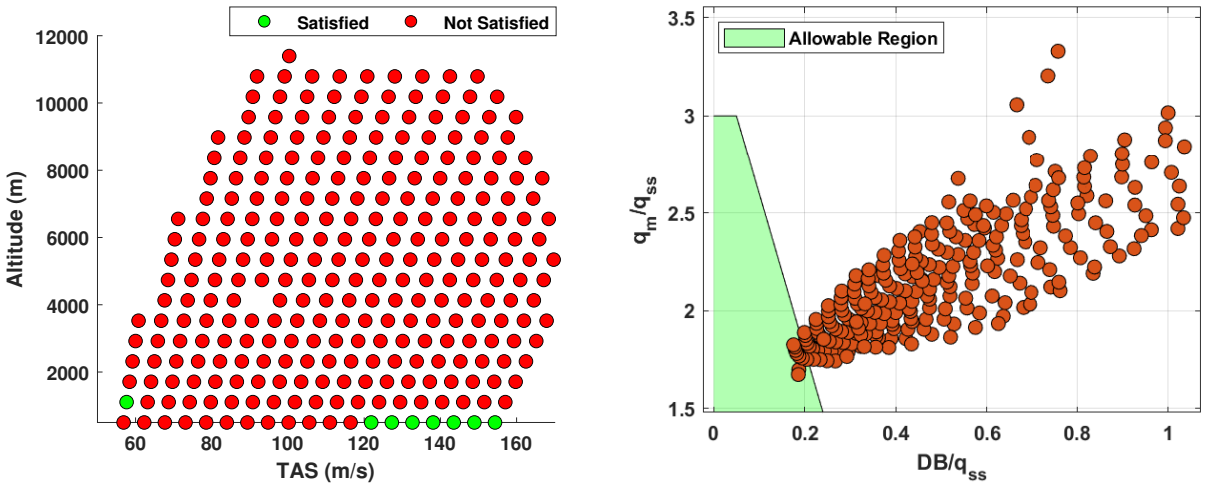

(a) Gibson criterion satisfaction across the trim envelope. **(b) Values of maximum pitch rate and dropback.**

Fig. 10 Gibson criterion satisfaction for the bare-airframe aircraft.

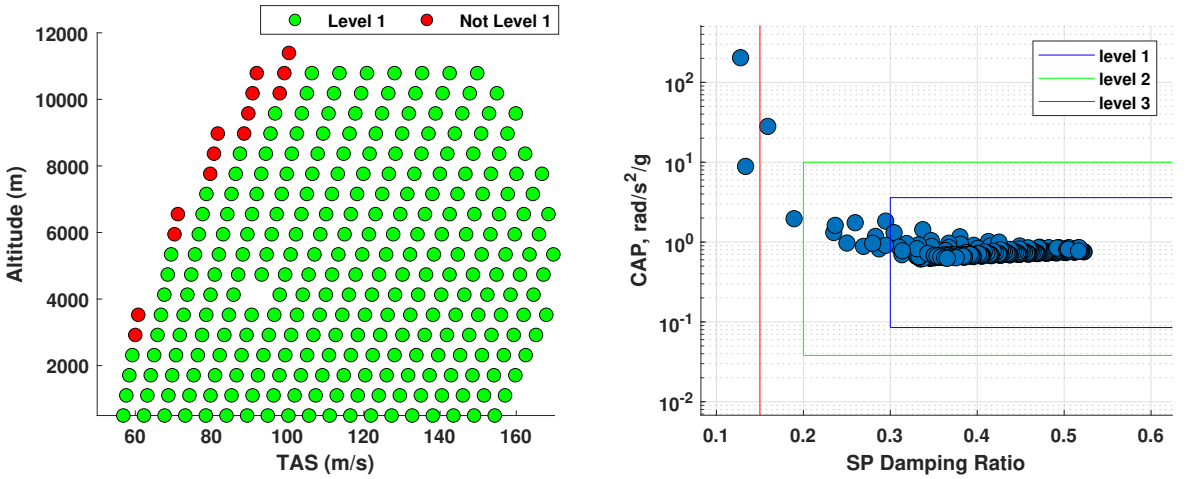

(a) CAP criterion satisfaction across the trim envelope. **(b) Values of CAP and short-period damping ratio.**

Fig. 11 CAP criterion satisfaction for the bare-airframe aircraft.

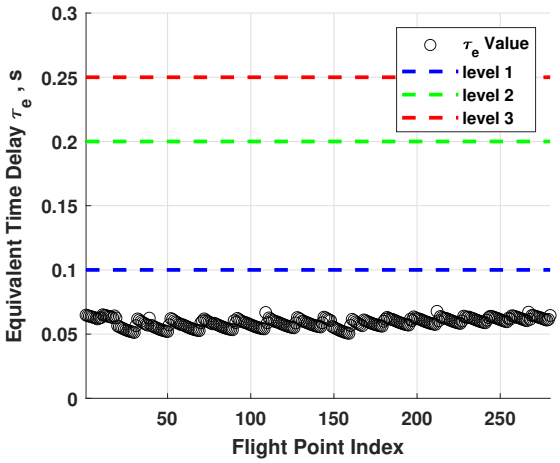

Fig. 12 Equivalent time delay values for bare-airframe aircraft.

IV. Control Law Design

A. Design Specifications

Table 3 lists the design specifications that will guide the design process. Achieving nominal performance involves meeting the three handling quality requirements, whereas nominal and robust stability are achieved by satisfying the generalized stability margin criterion. Robust performance will be assessed after the controller is implemented.

1. Design Point

Given the linear specifications, it is crucial to specify the flight condition (and as a consequence the linear model) where the controller will be designed. The selected flight condition aligns with the one chosen for comprehensive analysis of the bare airframe. For clarity and convenience, the conditions of this flight point are reiterated in Table 4.

Table 3 Design specifications.

Requirement	Source
CAP	(MIL-STD-1979A, 1990) [28]
Gibson Dropback Criterion	(Gibson, 1999) [29]
Equivalent Time Delay	(MIL-STD-1979A, 1990) [28]
Generalized Stability Margin ($\epsilon > 0.25$)	(McFarlane & Glover, 1992) [10]

Table 4 Design point data.

Height	TAS	Mach
3526 m	120 m/s	0.3684

2. Reference Model

To benefit from $\mathcal{H}_\infty$ control, the design specifications must be defined as bounds on the maximum or minimum singular values of the control system's various transfer functions and/or matrices. Therefore, obtaining a reference model T_{ref} that represents the handling quality specifications in the frequency domain is crucial for establishing the performance constraints. The CAP and Gibson criterion can be used to create the reference model by solving the following set of equations:

$$\begin{cases} \text{CAP} = \dfrac{g\omega_n T_{\theta 2}}{V_{TAS}} \\ \text{DB}/q_{ss} = T_{\theta 2} - \dfrac{2\xi}{\omega_n} \end{cases} \tag{19}$$

Table 5 presents the characteristic values of the obtained reference model. The CAP_{ref}, the $\text{DB}/q_{ss_{\text{ref}}}$, and ξ_{ref} values were picked from the level 1 and acceptable ranges of the handling qualities. With those values, it was possible to solve Eq. (19) and obtain ω_{ref} and $T_{\theta 2_{\text{ref}}}$. $K_{q_{\text{ref}}}$ was chosen such that T_{ref} has unitary static gain. Since the reference model is a pure second-order system, the equivalent time delay $\tau_{e_{\text{ref}}}$ is zero. Using the structure in Eq. (8), the reference model was generated. Finally, the value $q_m/q_{ss_{\text{ref}}}$ and the reference bandwidth value $\omega_{bw_{\text{ref}}}$ can be derived from the time and frequency responses of T_{ref}, respectively.

Table 5 Reference model characteristic values.

Variable	Value	Units
CAP_{ref}	0.5	rad/s^2/g
$\text{DB}/q_{ss_{\text{ref}}}$	0.15	-
ξ_{ref}	0.8	-
ω_{ref}	2.99	rad/s
$T_{\theta 2_{\text{ref}}}$	0.6849	-
$K_{q_{\text{ref}}}$	6.1302	-
$\tau_{e_{\text{ref}}}$	0	s
$q_m/q_{ss_{\text{ref}}}$	1.32	-
$\omega_{bw_{\text{ref}}}$	8.43	rad/s

B. Flight Control System Layout

The control system layout is depicted in Figure 13. As can be seen, the focus of this research will be a SISO system. The reduced aircraft model and the actuator have already been defined and constitute the plant G. The total controller K_{tot} is composed of the following four components:

- W_1 - pre-compensator to shape the open-loop gain;
- K_q - feedback controller to provide robust stability;
- K_{FF} - feedforward controller to provide handling quality satisfaction performance;
- k_{ref} - gain to ensure steady state reference tracking.

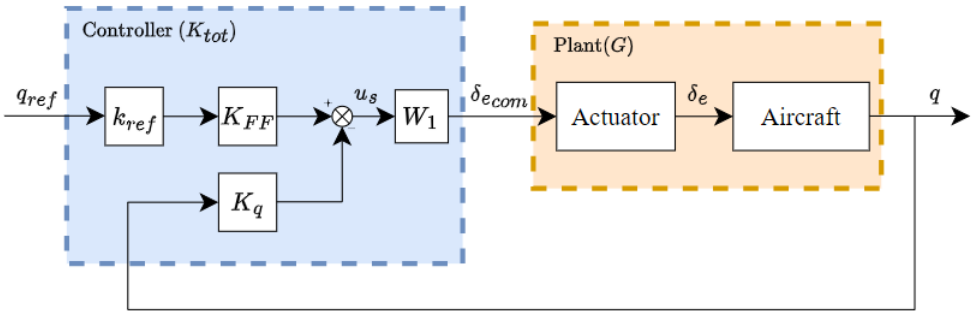

Fig. 13 Control system layout.

C. Loop-Shaping

The original theory [10] proposes tuning W_1 and W_2 compensators to do the loop-shaping. However, the decision here is to use only W_1. This approach makes the 2DoF design more straightforward since the outputs of the nominal and shaped plants will be the same. Moreover, in a SISO system, changes made before or after the plant yield the same effect on the open-loop gain due to the commutative property of multiplication. Therefore, this decision does not sacrifice any control over the loop shape.

Figure 14 shows the singular value plot of the nominal and shaped plants. To follow the guidelines of Section II.B.2, it was decided that W_1 would be of the form K_i/s. The gain K_i was adjusted so that the open-loop crossover frequency ω_c was similar to the closed-loop reference bandwidth of $\omega_{bw_{\text{ref}}} = 8.43$ rad/s, reflecting the relationship between these frequencies. The final pre-compensator is:

$$W_1 = \frac{5}{s} \tag{20}$$

D. One-Degree-of-Freedom Design

The one-degree-of-freedom (1DoF) problem provides valuable insight into the maximum obtainable generalized stability margin $\epsilon_{\max}$. Figure 15 shows the controller to be tuned along with the needed inputs and outputs to define the transfer matrix that will be part of the $\mathcal{H}_\infty$ problem. The relationship between the input and output is as follows:

$$\begin{bmatrix} y \\ u_s \end{bmatrix} = \begin{bmatrix} I \\ -K_\infty \end{bmatrix} (I + G_s K_\infty)^{-1} \begin{bmatrix} I & G_s \end{bmatrix} \begin{bmatrix} d_o \\ d_i \end{bmatrix} \tag{21}$$

and the goal is to find:

$$\epsilon_{\max}^{-1} = \inf_{K_\infty \text{stabilizing}} \left\| \begin{bmatrix} I \\ -K_\infty \end{bmatrix} (I + G_s K_\infty)^{-1} \begin{bmatrix} I & G_s \end{bmatrix} \right\|_\infty \tag{22}$$

The equivalence between Eq. (6) and Eq. (22) can be easily proven (see e.g. [10]). Using the *hinfstruct* routine in MATLAB, the nonsmooth optimization algorithm was employed to solve the problem for four different fixed-order K_∞ controllers. Table 6 gives the obtained maximum generalized stability margins. The value of $\epsilon_{\max}$ for K_∞ of order 1 is high enough to satisfy the design specification of $\epsilon > 0.25$. Hence, choosing this latter structure for the feedback controller K_q is anticipated to produce desirable results in the 2DoF design.

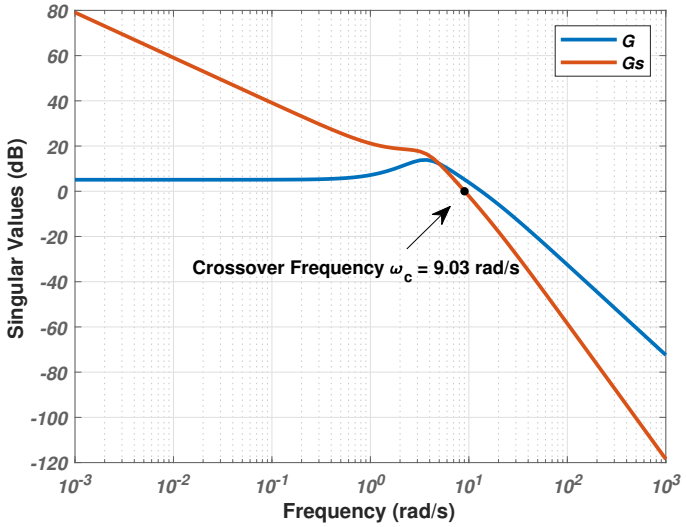

Fig. 14 Singular values of nominal and shaped plants.

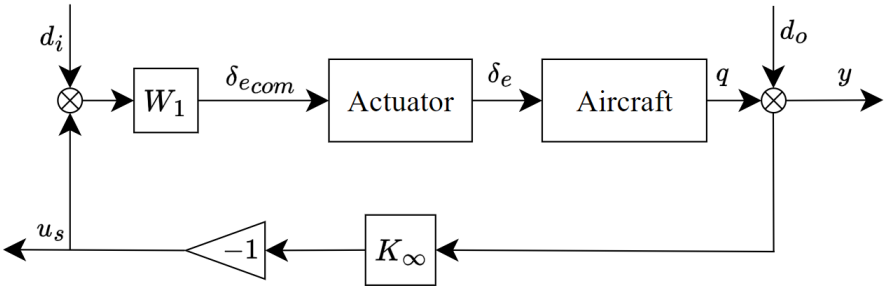

Fig. 15 1DoF $\mathcal{H}_\infty$ problem schematic formulation.

E. Two-Degree-of-Freedom Design

The transfer functions, inputs and outputs used for the final controller design are shown in Figure 16. The blocks K_{FF} and K_q are the tunable controllers for which a solution is required. The structure of K_{FF} is a transfer function composed of 3 zeros and 3 poles:

$$K_{FF} = \frac{k_{FF}(s+z_1)(s+z_2)(s+z_3)}{(s+p_1)(s+p_2)(s+p_3)} \tag{23}$$

and K_q is a first-order lead/lag compensator as defined by the one-degree-of-freedom problem:

$$K_q = \frac{k_q(s+z)}{(s+p)} \tag{24}$$

where $\{z_1, z_2, z_3, p_1, p_2, p_3\} \subset \mathbb{C}$ and $\{k_{FF}, k_q, z, p\} \subset \mathbb{R}$.

The final FCS should satisfy the requirements defined in Section IV.A. To this end, the handling qualities are considered through a soft constraint involving nominal performance, whereas a hard constraint is applied to ensure robust stability using the generalized stability margin. Additionally, a hard pole-placement constraint is imposed to prevent the closed-loop poles from having high frequencies, since that could lead to numerical problems.

Table 6 Controller order and respective maximum stability margin $\epsilon_{\max}$.

K_∞ Order	$\epsilon_{\max}$
4	0.3836
3	0.3836
2	0.3670
1	0.3189

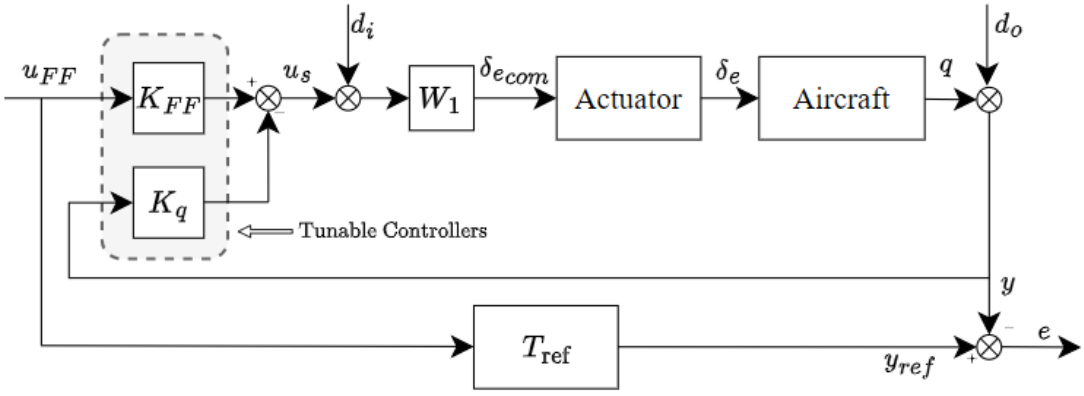

Fig. 16 2DoF problem layout.

1. Soft Constraint

The soft constraint concerns the reference model matching of the pitch rate q. Such behavior can be imposed through the use of the transfer function T_E, defined as follows:

$$e = T_E(s) \cdot u_{FF} \tag{25}$$

The constraint is hence written by:

$$S_1 : ||W_{S_1}(s)\ T_E(s)||_\infty < 1; \tag{26}$$

where $W_{S_1}(s)$ is a dynamic filter. The goal of the dynamic filter is to limit the reference matching to the relevant bandwidth. $W_{S_1}(s)$ was generated using $W_{S_1}(s)^{-1}$, since the inverse of the weighting function defines a desired upper bound on the magnitude of the transfer function it is applied to. $W_{S_1}(s)^{-1}$ was chosen to be a first-order high-pass filter of the following form:

$$W_{S_1}^{-1}(s) = \frac{c_1(s + c_2)}{s + c_3} \tag{27}$$

where the values of c_1, c_2, and c_3 can be obtain by choosing the static gain X, the high-frequency gain Y, and the gain Z at a specific frequency ω_Z, and solving

$$W_{S_1}^{-1}(0) = X \tag{28}$$

$$W_{S_1}^{-1}(\infty) = Y \tag{29}$$

$$|W_{S_1}^{-1}(j\omega_Z)| = Z \tag{30}$$

2. Hard Constraints

The first hard constraint H_1 will impose a generalized stability margin that can satisfy the design specifications. Using the common terminology of robust control, the relevant transfer functions for this constraint are defined as follows:

$$\begin{bmatrix} y \\ u_s \end{bmatrix} = \begin{bmatrix} S_s(s) & S_s(s)G_s(s) \\ -K_q(s)S_s(s) & -T_s(s) \end{bmatrix} \begin{bmatrix} d_o \\ d_i \end{bmatrix} \tag{31}$$

Using the information above, the constraint is formulated as:

$$H_1 : \left\| \begin{bmatrix} S_s(s) & S_s(s)G_s(s) \\ -K_q(s)S_s(s) & -T_s(s) \end{bmatrix} \right\|_\infty < \epsilon_s^{-1} \tag{32}$$

with ϵ_s being the imposed generalized stability margin.

The second hard constraint H_2 concerns the clustering of the closed-loop poles inside a disk $\mathcal{D}$ centered at the origin and with a radius $r = \omega_{max}$. Such constraints can be formulated using a Linear Matrix Inequalities (LMI) approach [34]. A subset $\mathcal{D}$ of the complex plane is called an LMI region if there exists a symmetric matrix $\alpha \in \mathbb{R}^{m\times m}$ and a matrix $\beta \in \mathbb{R}^{m\times m}$ such that:

$$\mathcal{D} = \{z \in \mathbb{C} : \quad f_{\mathcal{D}}(z) < 0\} \tag{33}$$

with $f_{\mathcal{D}}(z) := \alpha + z\beta + \bar{z}\beta^T$. For the definition of the constraint, the closed-loop transfer function T_q needs to be obtained as follows

$$q = T_q(s) \cdot u_{FF} \tag{34}$$

Defining:

$$f_{\mathcal{D}}(z) = \begin{bmatrix} -\omega_{\max} & z \\ \bar{z} & -\omega_{\max} \end{bmatrix} \tag{35}$$

which clearly aligns with the requirements for defining an LMI region, the closed-loop transfer function T_q has to respect the following structural constraint:

$$H_2 : \quad \forall p'_i \in p'_1, p'_2, \ldots, p'_n, \quad p'_i \in \mathcal{D}, \tag{36}$$

where $\{p'_1, p'_2, \ldots, p'_n\}$ represents the set of all poles p'_i of T_q.

3. Obtained Solution

The objective is to find stabilizable controllers K_q and K_{FF} that minimize the soft constraint S_1 and satisfy the hard constraints H_1 and H_2. To perform the described optimization, the nonsmooth optimization algorithms were employed through the tunning command *systune* available in MATLAB. Additionally, the SLTuner tool was used to provide an interface between Simulink, where the control system architecture was defined, and *systune*. The obtained solution is as follows:

$$K_{FF} = \frac{-25.948(s + 0.8676)(s^2 + 3.13s + 78.05)}{(s + 50)(s + 43.92)(s + 2.394)} \tag{37}$$

$$K_q = \frac{-2.9813(s + 4.019)}{(s + 35.72)} \tag{38}$$

$$k_{\text{ref}} = T_q^{-1}(0) = 1.0034 \tag{39}$$

with:

$$\epsilon = 0.3180 \approx \epsilon_{\max} = 0.3189 \tag{40}$$

As Eq. (40) demonstrates, the obtained value of ϵ is approximately the maximum achievable $\epsilon_{\max}$ for a lead-lag K_q. This result means that no robust stability was sacrificed in order to obtain performance.

V. Theoretical Analysis of the Control Law

A. Gap Metric and Stability Region

The gap metric was introduced into the control literature by [35] as being appropriate for the study of uncertainty in feedback systems. This metric defines notions of distance in the space of (possibly) unstable systems which need not necessarily have the same number of RHP poles. The problem of robustness optimization in the gap metric is equivalent to robustness optimization for normalized coprime factor perturbations [36].

Hence, using the $\mathcal{H}_\infty$ loop-shaping algorithm to maximize allowable coprime factor uncertainty corresponds to tolerating the largest ball of uncertainty in the gap metric. If $P1 = N_1 M_1^{-1}$ and $P2 = N_2 M_2^{-1}$ are normalized right coprime factorizations, then the gap metric δ_g is as follows:

$$\delta_g\left(P_1, P_2\right) = \max\left\{\vec{\delta}\left(P_1, P_2\right), \vec{\delta}\left(P_2, P_1\right)\right\} \tag{41}$$

where $\vec{\delta}_g$ is the directed gap and can be computed by:

$$\vec{\delta}_g\left(P_1, P_2\right) = \inf_{Q \in \mathcal{H}_\infty} \left\| \begin{bmatrix} M_1 \\ N_1 \end{bmatrix} - \begin{bmatrix} M_2 \\ N_2 \end{bmatrix} Q \right\|_\infty \tag{42}$$

The two following expressions that use the variables introduced in Eq. (4) are equivalent:

$$\delta_g(G, G_p) < \epsilon \tag{43}$$

$$\left\| \begin{pmatrix} \Delta_M \\ \Delta_N \end{pmatrix} \right\|_\infty < \epsilon \tag{44}$$

This relation makes it possible to translate the obtained ϵ into a region of guaranteed stability around the nominal design point. Figure 17 shows this region.

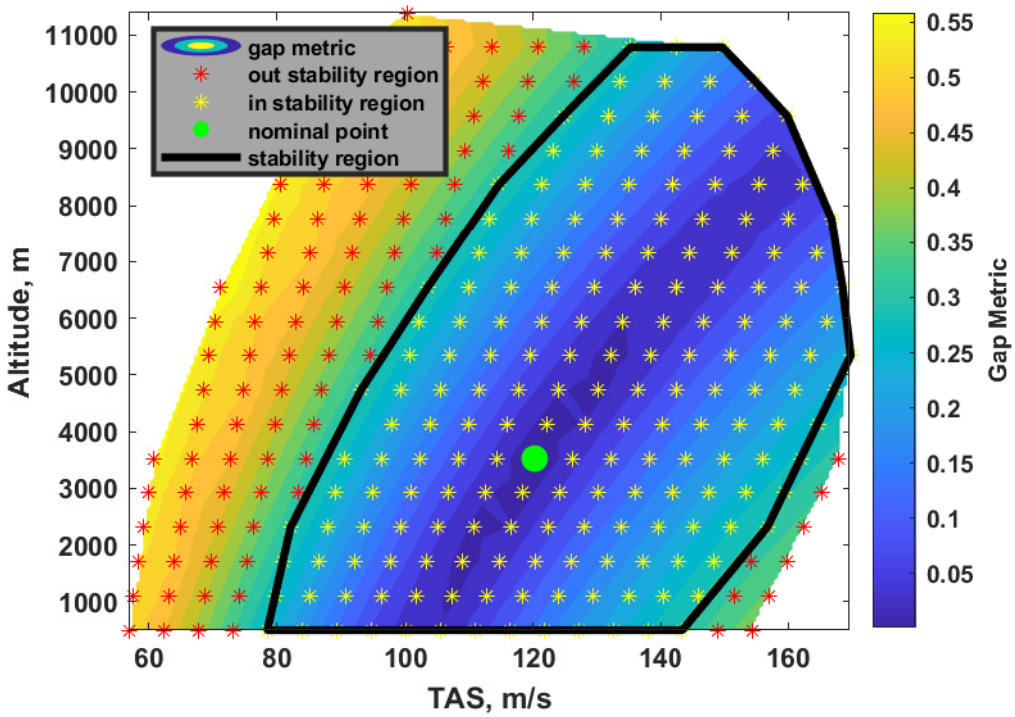

Fig. 17 Guaranteed stability region obtained through the gap metric.

B. Closed-Loop Analysis

In order to analyze the obtained control law the following results are given. In all the figures mentioned in this paragraph, the blue curves are related to the non-nominal flight points inside the guaranteed stability region. Figure 18 illustrates the singular values of the open-loop transfer function, contrasting the nominal and non-nominal stabilized plants ($G_{stab} = G_s K_q$) with the shaped plant. The influence of K_q is evident as it reduces the roll-off rate around the crossover frequency. This phenomenon has been known for a long time to be closely related to close-loop stability

in SISO systems. In addition, it can also be verified that the obtained value of $\epsilon = 0.318$ is high enough so that little deterioration between the shaped and stabilized plants is seen. Figure 19 gives the singular values of key closed-loop functions. S and T refer to the sensitivity and complementary sensitivity functions of the system with plant G and controller $K = W_1 K_q$. It can be concluded that the levels of disturbance rejection and actuator deflection are satisfactory and remain acceptable for the entire range of models. Figure 20 is the Nichols diagram and the obtained S-T-based exclusion region. As expected, the guaranteed phase and gain margins of $\mathcal{H}_\infty$ loop-shaping provided excellent levels of robustness against pure phase, pure gain, and simultaneous phase and gain perturbations at the input or output of the plant. Lastly, Figure 21 shows the nominal, the non-nominal, and the reference pitch rate step responses. The reference model is closely matched, showing the effect of constraint S_1.

C. Theoretical Analysis of Handling Qualities

It has already been visually concluded that the pitch rate and the reference model step response are well-matched. Nevertheless, the question remains of whether robust performance has been achieved. To evaluate if this is the case, Figure 22 presents a handling quality analysis for the flight points inside the guaranteed stability region. It can be seen that the handling qualities are satisfied for almost the entire region. The exception are four flight points at high altitudes close to the boundaries of the stability region. Notwithstanding, this is a considerably high level of robust performance. The design of the control law is finished.

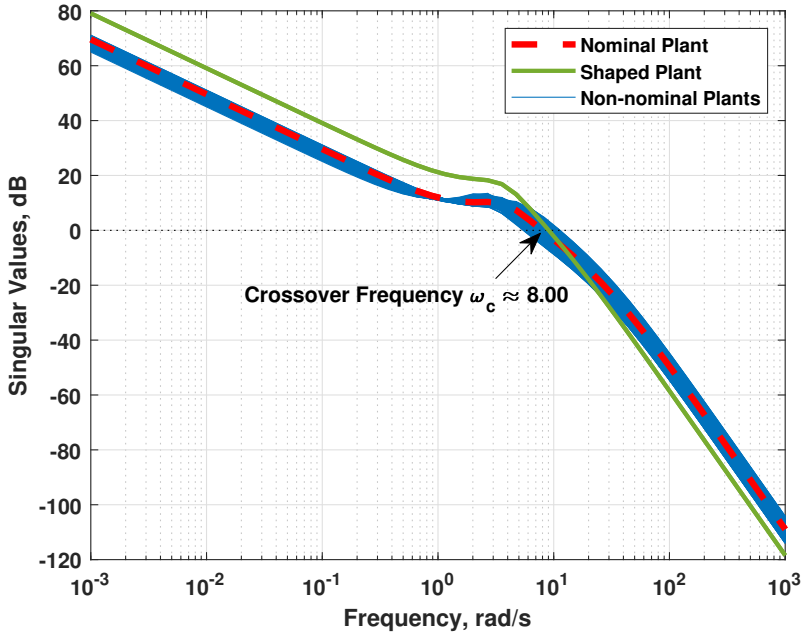

Fig. 18 Open-loop singular values.

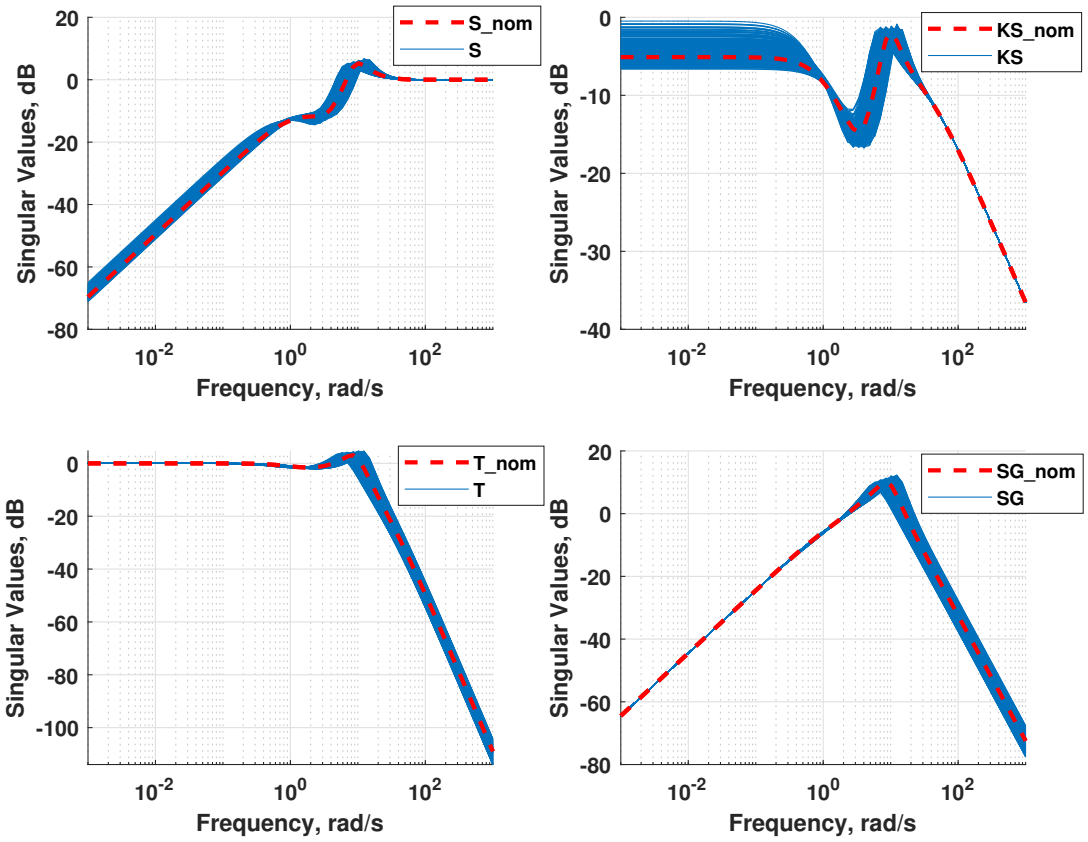

Fig. 19 Closed-loop singular values.

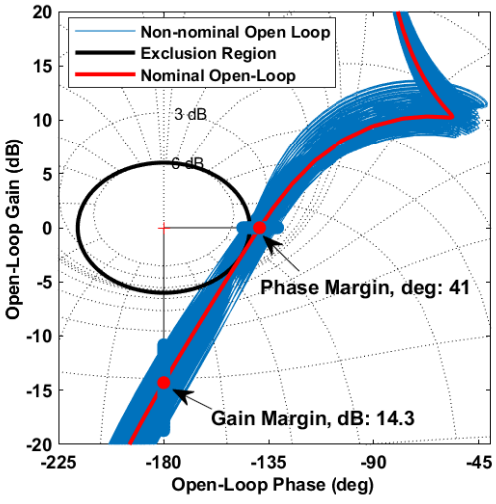

Fig. 20 Nichols plot and exclusion regions.

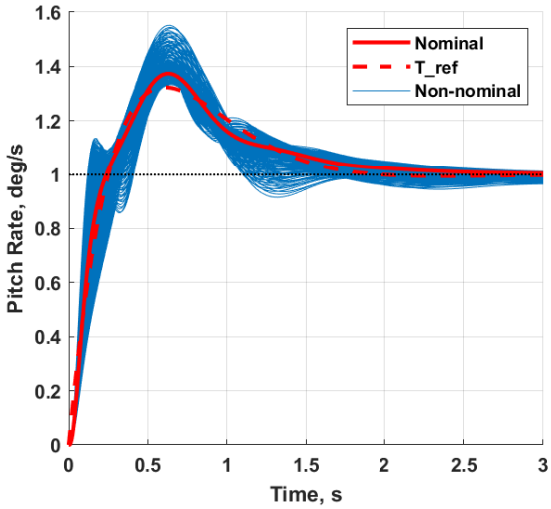

Fig. 21 Pitch rate step response.

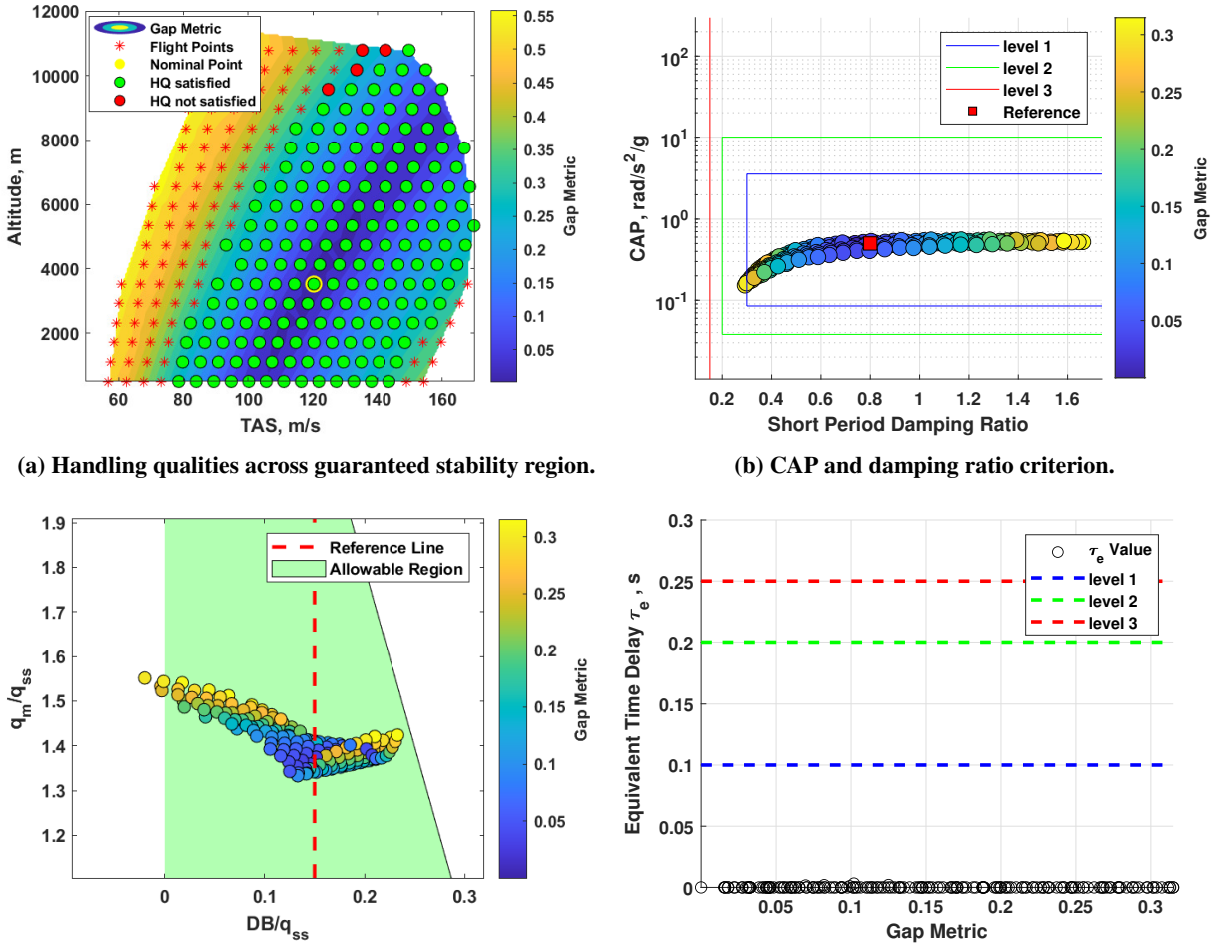

(a) Handling qualities across guaranteed stability region.

(b) CAP and damping ratio criterion.

(c) Gibson dropback criterion.

(d) Equivalent time delay criterion.

Fig. 22 Theoretical handling qualities analysis of the closed-loop.

VI. Simulator Evaluation of the Control Law

A. Objectives

The first objective of the simulation experiment is to evaluate the handling qualities of the bare airframe. This will provide a baseline understanding of how the aircraft performs naturally, offering a reference point for comparison with the case where the aircraft is equipped with a control system. The second objective is to experimentally validate the promising results achieved by the designed control law. More specifically, the ability to satisfy handling qualities across a large portion of the guaranteed stability region. The third and last objective is to investigate whether the augmented airframe (closed-loop system) has better handling qualities than the bare airframe. If this is the case, it would be confirmed that the implemented CAS can improve the baseline handling qualities of the aircraft. This improvement should be evident in considerably different flight conditions across the guaranteed stability region.

B. Configurations and Flight Conditions

It logically follows from the objectives that two aircraft configurations will be tested: the bare-airframe aircraft and the aircraft augmented with the RCAH system. The plan for this simulator campaign is to execute maneuvers in the three flight conditions shown in Table 7. The table lists indicated airspeed (IAS), true airspeed (TAS), altitude in both feet and meters, Mach number, and mass for each of the three flight conditions evaluated: slow/low, moderate, and fast/high. These flight conditions were selected to validate the robustness performance results of the designed controller. Each condition varies considerably in altitude and speed. Notwithstanding, these conditions remain within the guaranteed stability limits.

Table 7 Flight conditions.

Flight Condition	IAS (kts)	TAS (m/s)	Altitude (ft)	Altitude (m)	Mach	Mass (kg)
1 (slow/low)	167.41	90.77	3625	1105	0.270	5000
2 (moderate)	197.15	120.28	11568	3526	0.368	5000
3 (fast/high)	228.19	161.96	21496	6553	0.515	5000

C. Setup

The entire simulation is to be performed with the autothrottle on. The trim speed is the autothrottle reference and is set automatically. The pilots cannot change the autothrottle reference. The motivation for the autothrottle use is to let the pilots focus only on the elevator/pitch rate commands (depending on the configuration) and ensure the aircraft remains close to the trimmed flight point. With the autothrottle off, there is the risk of the pilots losing track of the airspeed and ending up far away from the initial flight point and even outside the guaranteed stability region. This way, similar conditions between configurations can also be more easily obtained. Even though the real bare-airframe aircraft does not have an autothrottle, one is included in the simulation for the mentioned reasons.

As expected, the simulation experiment only covers longitudinal maneuvers. Additionally, the maneuvers do not involve disturbance rejection since no wind or turbulence was introduced. The selected control inceptor is the sidestick. Hence, for all simulation runs the pilot only needs to focus on the sidestick. Further, lateral deflections of the sidestick are allowed but do not cause any effect. In the bare airframe configuration, the sidestick automatically moves to the trim position at the beginning of every run. Other available hardware such as the pedals, the throttle levers, and the mode control panel are not to be used. Lastly, the throttle levers do not respond to the autothrottle commands and therefore remain stationary throughout the experiment.

1. Head-Up Display

The primary flight display of the simulator cockpit is used to present the pilot with available aircraft information in a head-up display (HUD) alike, green on black, layout. This includes velocity, Mach number, thrust lever setting and output, pitch angle, flight path angle, angle of attack, sideslip angle, and altitude. Figure 23 shows the default configuration of the HUD. The image is presented in greyscale for improved clarity. Depending on the task, additional information such as scores and references to follow are added to this baseline version of the HUD.

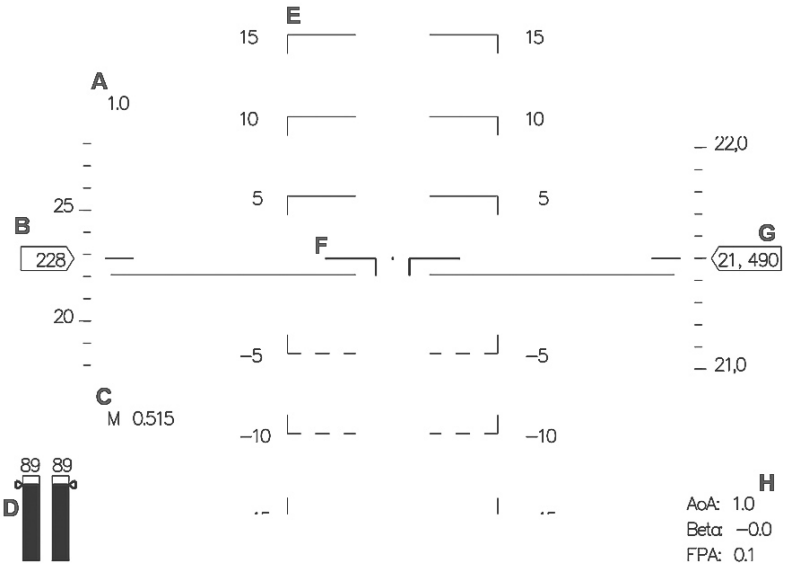

Fig. 23 Default HUD with A: load factor (g); B: IAS (kts); C: Mach number; D: power lever setting (triangle) and thrust level (% max level); E: pitch angle ladder (deg); F: pitch angle indicator (deg); G: altitude (ft); H: angle of attack, sideslip angle, and flight path angle (deg).

2. Stick Dynamics and Gearing

For the bare airframe, it was decided to use linear gearing where zero stick deflection δ_s corresponds to zero elevator position. Table 8 shows the minimum and maximum possible deflections of the actuator.

Table 8 Minimum and maximum actuator deflections.

Minimum Deflection	Maximum Deflection
-20^o	15^o

To keep the linear relation, the selected range of possible commanded values of δ_e is $[-15, 15]$ deg. Assuming the maximum sidestick deflection is 18 deg, the relation between sidestick deflection and commanded elevator deflection is as presented below:

$$\frac{\delta_{e\,com}}{\delta_s} = \frac{15}{18} \tag{45}$$

Simulations were used to choose the gearing for the aircraft augmented with the RCAH system. Ultimately, it was stipulated that the range of possible commanded q is $[-15, 15]$ deg/s. This range should allow the pilot to require a maximum load factor of around 4 g and a minimum of -1.5 g. With this gearing, the relation between stick deflection and commanded pitch rate is as follows:

$$\frac{q_{com}}{\delta_s} = -\frac{15}{18} \tag{46}$$

The sidestick makes use of a control loading mechanism to set the stiffness (k_s), damping (b_s), and inertia (m_s) parameters of the sidestick. These parameters are used to create the stick dynamics. By applying the pitch rate sensitivity criterion [29], it is possible to obtain values for the function $\frac{\delta_{com}}{F_e}$ that governs the relation between the force F_e exerted by the pilot on the stick - measured at the stick's reference point, located at the bottom of the trigger button - and the commanded elevator deflection or pitch rate δ_{com}, depending on the configuration. The relation between the latter function and the stick dynamics $\frac{\delta_s}{F_e}$ is as follows:

$$\frac{\delta_{com}}{F_e}(s) = \frac{\delta_s}{F_e}(s) \cdot \frac{\delta_{com}}{\delta_s} \tag{47}$$

Since the gains to convert the stick deflection into the commanded δ_e or q have already been defined, it is possible to generate values for the stick parameters. In this case, it was decided to implement a Q-feel system. Therefore, as the dynamic pressure increases the force needed to move the sidestick increases as well. In the bare airframe, the goal is to recreate the additional resistance the pilot would find to control the elevator at higher speeds. In the augmented aircraft, such strategy is justified by the need to anticipate to the pilot the effects of their own command demand.

Table 9 shows the bare airframe stick dynamics for different flight conditions. As can be seen, in the high and fast flight condition the pilot will need almost twice the force to cause the same elevator deflection as in the low and slow flight condition. Table 10 shows the augmented aircraft stick dynamics for different flight conditions. The pitch rate that 1 lbf can produce reduces with the speed. This is once again an effect of the artificial feel system. Additionally, there is a breakout force to ensure that zero stick deflection commands zero pitch rate.

Table 9 Flight condition and stick dynamics for bare airframe.

Flight Condition	m_s (Ns^2/deg)	b_s (Ns/deg)	k_s (N/deg)	q_m/lbf (deg)	δ_e/lbf
1 (slow/low)	0.015	0.500	13.33	0.83	0.276
2 (moderate)	0.015	0.500	17.5	0.75	0.212
3 (fast/high)	0.015	0.500	24.17	0.6144	0.153

Table 10 Flight condition and stick dynamics for augmented aircraft.

Flight Condition	m_s (Ns^2/deg)	b_s (Ns/deg)	k_s (N/deg)	q_m/lbf (deg)	Breakout Force (N)
1 (slow/low)	0.003	0.221	5	1.04	4.5
2 (moderate)	0.003	0.221	6.67	0.76	4.5
3 (fast/high)	0.003	0.221	7.92	0.62	4.5

3. Motion

Motion filters are essential for converting the movement of the aircraft into motion cues while respecting the physical constraints of the motion system. To tune the filters, an experimental approach was used. The relevant maneuvers were replayed in the simulator for different sets of parameters. The goal was to provide maximal cueing without ever breaching the position, velocity, and acceleration limits of the simulator. Since only longitudinal maneuvers were tested, motion filtering was only done for the surge, heave, and pitch. Table 11 presents the order of the used motion filter along with the final values of the parameters.

Table 11 Motion parameters.

	High-pass filter					Low-pass filter		
DOF	Ord.	K	ω_n (rad/s)	ζ	ω_b (rad/s)	Ord.	ω_n (rad/s)	ζ
surge (x)	2nd	0.7	0.7	0.7	-	2nd	1.2	0.7
sway (y)	-	-	-	-	-	-	-	-
heave (z)	3rd	0.4	2	0.7	0.2			
roll (φ)	-	-	-	-	-			
pitch (θ)	2nd	0.7	0.7	0.7	-			
yaw (ψ)	-	-	-	-	-			

D. Selection of Maneuvers

Maneuver design and selection are based on the *MIL-STD-1797A* [28]. Together, these tasks are designed to examine the two most critical longitudinal types of control: attitude and flight path control. The following sections describe the tasks in more detail.

1. Pitch Tracking

The pitch tracking task consists of tracking a pitch angle reference signal to achieve the desired performance (defined in the following lines) while following the recommended control approach. For this maneuver, a reference signal that is made up of steps and ramps is generated. Starting from the trim condition, the pilot is asked to follow the pitch angle reference for 76 to 80 seconds depending on the flight condition. The reference to follow is shown in the HUD display. The desired margin is defined by $\pm 0.5^o$ from the reference signal, whereas it is $\pm 1^o$ for the adequate margin. The HUD will represent these margins with a small (desired) and a large (adequate) square as demonstrated in Figure 24a. The HUD will display two percentages during this task, representing the adequate and desired performance scores. The desired performance score reflects the percentage of time the pilot has spent inside the desired margin (the small square). Following the same logic, the adequate performance score reflects the percentage of time the pilot has spent inside the adequate margins (the large square). To meet the desired and adequate performance, the pilot must achieve at least 80% of the respective performance score. This value was determined through experimental iterations, gradually increasing the pilot's gain and assessing the resulting performance score. A threshold of 80% was identified as striking the optimal balance: it stresses the aircraft sufficiently to reveal any existing deficiencies while avoiding extremely unrealistic levels of aggressiveness.

2. Flight Path Tracking

In essence, the layout of this task is very similar to that of the pitch angle tracking experiment. The only difference is that the reference to be followed uses the flight path angle instead of the pitch angle. The desired and adequate margins and the performance scores will also appear in the HUD display. This time, however, the margins are represented by dashed lines instead of squares as seen in Figure 24b. The margins have the same values as in the pitch tracking task. To meet the desired and adequate performance, the pilot must achieve at least 75% of the respective performance score. This value was determined using the same strategy as the previous task.

3. Pitch Capture

Pitch captures start with the aircraft trimmed according to a specific flight condition. Then, the pilot is asked to perform a series of pitch captures of 3^o increments in both directions. This process is then repeated for increments of 6^o. The pilot will see a reference in the HUD indicating the pitch angle they should capture. Once again, squared margins indicate the desired and adequate intervals where the pitch angle reference should be. The reference stays visible long enough so the pilots can do the captures at their own pace. No scores are shown in this task. The pilots' comments should be enough to understand and evaluate the control law.

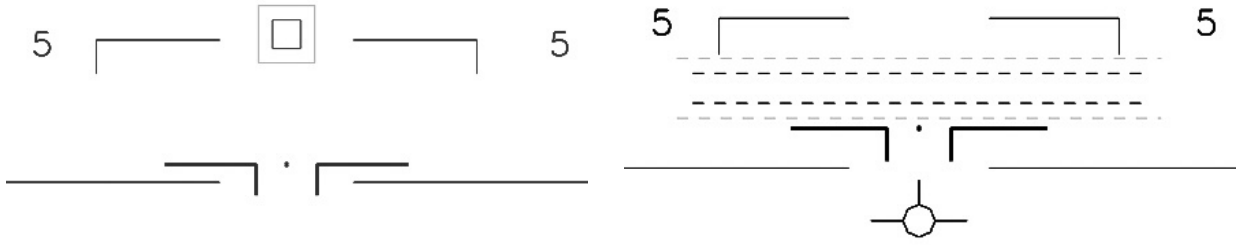

(a) Pitch tracking and pitch capture HUD detail. **(b) Flight path tracking HUD detail.**

Fig. 24 Different configurations of the HUD.

E. Methodology

1. Testing Methodology

From the necessity of creating a quantitative measure instead of only relying on the pilots' subjective impression when analyzing handling qualities, the Cooper-Harper handling qualities rating scale was introduced [27]. The goal of this scale is to standardize the process of handling quality evaluation. A usual abbreviation of the Cooper-Harper scale is HQR, for handling qualities rating. This flight-testing campaign uses this approach. Nevertheless, a rating means nothing without explanatory comments. Therefore, it is essential to also provide the testing pilots with the opportunity to be critical about the response of aircraft and note down their opinions. Finally, another important measure of the aircraft characteristics is the type of performance (adequate or desired) that is achieved.

Combining all the tasks, flight conditions, and configurations, a total of $3 \times 3 \times 2 = 18$ scenarios are to be tested. Each scenario takes several simulation runs to complete (usually between 1 and 3). After each simulation run, the pilot is asked for comments. Subsequently, depending on the will of the pilot the run can be repeated or not. If not, the HQR is given (tracking tasks only) and any final comments are noted. Once this step is done, the experiment moves on to the next scenario.

2. Recommended Control Approach

The pilots are asked to fly the tasks as they would in a passenger aircraft, with the possibility of being somewhat more aggressive to emulate their actions, for example, in an emergency situation where passenger comfort could be slightly disregarded. The control approach should always be a realistic one considering the Cessna Citation II is a passenger aircraft. In general, it is recommended to try to maintain the load factor between 1.3g and 0.7g. If the pilots want to test a different level of aggressiveness or control approach this can be communicated and a dedicated simulator run shall be used to test such strategy.

F. Hypotheses

From the experiment objectives, configurations, and selection of tasks, it is possible to formulate hypotheses that reflect the expected results. These are based on the conclusions from Sections III and V. The bare-airframe aircraft is expected to achieve adequate or desirable performance in the pitch tasks. The aircraft response will be bobbly and the tasks will always be performed with a certain degree of pilot compensation. The flight path tracking task will always achieve desirable performance. Since the pilot does not control the flight path directly, some compensation is expected. The augmented aircraft is expected to always achieve desirable performance in the pitch tasks. The aircraft response will be satisfactory and little pilot compensation should be necessary. The flight path tracking task will always achieve desirable performance. Since the pilot does not control the flight path directly, some compensation is expected. Lastly, it is hypothesized that the augmented aircraft will have better handling qualities than the bare airframe for the pitch tasks. This improvement will be seen in all three flight conditions. The flight path tracking task will have similar handling qualities between the two configurations.

G. Results

The experiment was carried out by two pilots, both with the research test pilot credential. To keep their identification private, they will be referred to as pilots 1 and 2. Moreover, the following terminology will be used in the exposure of the results:

- BA (bare airframe), AA (augmented aircraft);
- FC (flight condition).

1. Pitch Tracking

The pilots were first asked to accomplish the pitch tracking task. Figure 25 displays the performance scores obtained by both pilots. It is evident that the augmented aircraft consistently achieved the desired performance. In contrast, the bare-airframe aircraft failed to meet the defined minimum desired score for pilot 1 in FC2. The primary focus is on whether the desired performance was achieved, rather than on the relative scores between different configurations. This is because the pilots were instructed to use a realistic approach not to maximize their performance. Typically, pilots repeat runs until the appropriate performance level has been achieved. In some instances, pilots achieved the minimum required score of 80% on their first try. In other cases, they missed by 1% but significantly surpassed the target score on

their second attempt due to increased familiarity with the aircraft's response. Therefore, relative scores are irrelevant due to the nature of the experimental design. Additionally, adequate performance was always easily achieved demonstrating that the controllability of the aircraft was never in question during the experiment. Figure 26 shows the HQR given by the pilots for each configuration and flight condition. The bare airframe received ratings between 1 and 4. Specifically, pilot 1 never gave a rating of 1, and pilot 2 only did so for FC1. These results suggest that the pilots often had to compensate for certain characteristics of the bare-airframe aircraft, particularly in the scenarios where the HQR was 3 or 4. In contrast, the augmented aircraft always received an HQR of 1, indicating an excellent response with no need for pilot compensation to achieve the desired performance. The pilots' main points are summarized in the following list:

- **Workload:** Both pilots agreed that doing the task with bare airframe was demanding. Pilot 1 noted that the task required significant concentration, particularly finding FC3 the most difficult to control. He also mentioned that he would not want to regularly perform the given task using an aircraft with these characteristics. Pilot 2 remarked that he used anticipation and strategy to complete the task, especially in FC3 for which he needed an increased focus. In contrast, the pilots experienced a reduced workload with the augmented aircraft. Pilot 1 commented that the task felt almost too easy, like "cheating." Pilot 2 agreed, stating that there was nothing wrong with the response.
- **Aircraft Response:** The pilots observed noticeable differences in aircraft response between configurations. Pilot 1 noted a tendency to oscillate with the bare airframe, which he nevertheless found manageable, whereas Pilot 2 described the response as "sloppy and low-damped." In contrast, with the augmented airframe, Pilot 1 perceived the response as smooth and precise. Further, pilot 2 commented that he experienced a sharp and clear response, adding that he could simply "point and shoot."
- **Control Strategy:** Both pilots adopted a more aggressive approach than they would in a typical passenger flight, recognizing that their usual level of aggressiveness was not conducive to achieving desirable performance. Pilot 1 initially performed the task by selecting the pitch rate and then releasing the stick upon meeting the target. However, he later found a more effective approach by slightly decreasing the gain as he approached the target. Similarly, Pilot 2 initially attempted the task while monitoring load factor and score indications in the HUD. However, after several attempts, he abandoned this approach in favor of focusing solely on the tracking task, which yielded better results with reduced workload.
- **Flight Conditions:** In the bare airframe, both pilots clearly felt the different dynamics as they were moving from low altitude and speed to higher ones. FC3 was pointed out as having the more challenging dynamics. In the words of pilot 1, FC3 was less damped than the other conditions. As mentioned previously, pilot 2 felt a substantial increase in workload once he got to FC3, compared to the other conditions. In the augmented airframe, the pilots felt no differences between flight conditions.
- **Forcing Functions:** The forcing function of FC2 was deemed by both pilots as being more challenging than the others. Pilot 1 said that there were more steps and that the reversions were causing more oscillations. Agreeing with him, Pilot 2 commented that there were more pitching up to pitching down changes that required him to be more aggressive, conflicting with passenger comfort.

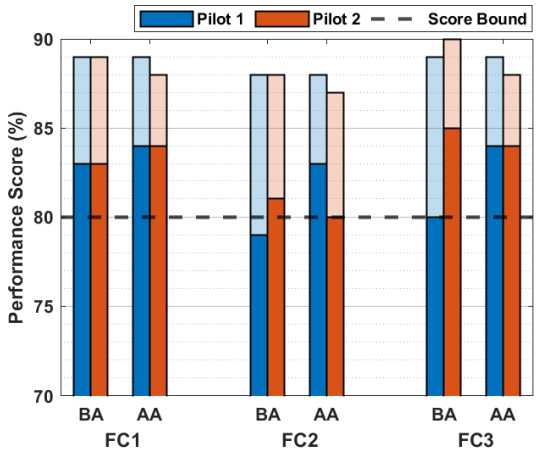

Fig. 25 Performance score for pitch tracking task. Opaque bars are the desired performance score and transparent bars are the adequate performance score.

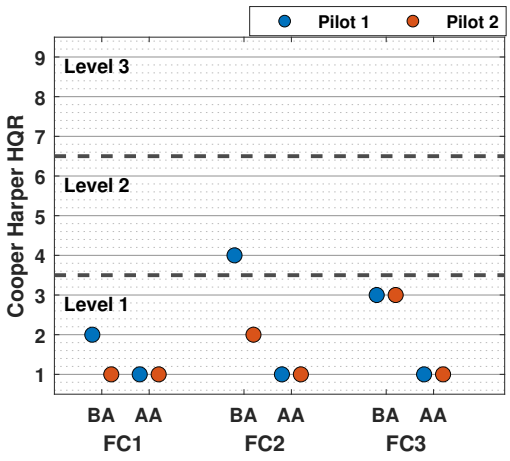

Fig. 26 HQR for pitch tracking task.

2. Flight Path Tracking

The second task the pilots performed was the flight path tracking. Figure 27 shows the performance scores attained by each pilot in this task. In all cases, the desired performance was achieved. Figure 28 presents the Cooper Harper HQRs given by the pilots in the different flight conditions. The HQRs for both pilots always fell within Level 1, except for the BA configuration in FC3 with Pilot 1. In general, however, there is no clear distinction between the distribution of HQRs for the two configurations. Pilot 1 tended to give lower (better) HQRs for the augmented aircraft configuration, whereas Pilot 2 showed a tendency to rate the bare airframe configuration more favorably. Therefore, despite both pilots achieving the desired performance scores, these last results indicate individual preferences and perceptions of the aircraft handling qualities under different configurations. The comments of the pilots during this task allow the following conclusions to be made:

- **Aircraft Response:** The general feeling was that in both configurations the flight path response had a delay in relation to the pilot input. The pilots expressed this idea using expressions such as "I have to anticipate more." Pilot 1 also talked about the fact that he was controlling a different variable than the one he was tracking, making the experienced delay expected.
- **Flight Condition:** Flight condition differences in the flight path response were noticed by the pilots in both configurations. In the bare airframe, Pilot 2 felt the task was becoming easier as he went from FC1 to FC3. In his opinion, the change in the dynamics of the aircraft was helping the task, making the response less inconsistent and more precise. Nevertheless, the pilot questioned whether this feeling could be a result of him getting adapted to the flight path response. In this particular aspect, Pilot 1 felt the exact opposite way, stating he was overshooting more and experiencing more oscillations as the altitude and speed increased. In the augmented aircraft, Pilot 1 felt the task was becoming more difficult as the altitude and speed increased.
- **Adaptation:** Both pilots think that with more time to get used to the flight path response, the task would become easier. Pilot 1 stated that with more practice time, the augmented aircraft would probably be rated with a HQR of 1. Pilot 2 mentioned that after many hours, he would expect this tracking task to be less challenging.
- **Control Strategy** Both pilots affirmed they were anticipating the sluggish response of the flight path in order to obtain the desired performance.
- **Possible Improvements:** Pilot 1 preferred the boxes instead of the dashed lines, as the way to indicate the desired and adequate margins in the HUD. Additionally, he found the display slightly cluttered in FC3, since the angle of attack was lower and hence the pitch angle indicator and the flight path marker were sometimes overlapping. Lastly, this same pilot mentioned that he found it unlikely that the specific flight path changes being tracked would be required during an actual flight.

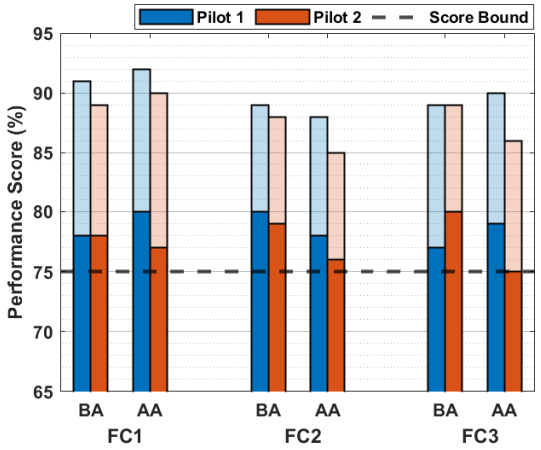

Fig. 27 Performance score for flight path tracking task. Opaque bars are the desired performance score and transparent bars are the adequate performance score.

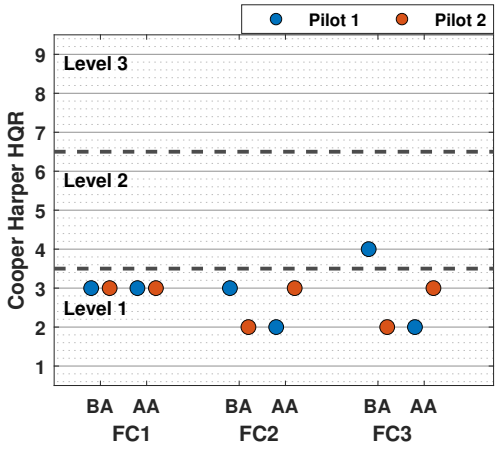

Fig. 28 HQR for flight path tracking task.

3. Pitch Capture

The final task performed was the pitch capture. In this case, for each flight condition, the pilots evaluated the configurations consecutively and were then asked to indicate their preferred choice. Across all conditions, the pilots consistently preferred the augmented aircraft. This task also provided an opportunity to evaluate the aircraft without the pressure of meeting a minimum score requirement. Consequently, the pilots were able to adjust their gains and focus more closely on the characteristics of both configurations. It also served as a chance to assess whether favorable handling qualities observed in the pitch tracking task were consistent in the pitch capture. The comments provided by the pilots can be categorized as follows:

- **Workload:** The reduced workload associated with attitude tasks in the augmented aircraft was further emphasized. Pilot 1 reiterated that this specific configuration was significantly easier to control, expressing a clear and definite preference for its response. While Pilot 2 was less emphatic, he also indicated a preference for the aircraft equipped with the RCAH system. Pilot 2 noted that the bare airframe necessitated continuous input to maintain a captured attitude, rather than simply releasing the stick.
- **Control Strategy:** In the first tries the pilots were excessively aggressive. After communication with the control room, they adopted a more realistic gain. For the bare airframe, Pilot 2 reported employing multiple adjustments to remain close to the reference attitude. In contrast, for the augmented aircraft, Pilot 1 indicated that he was able to control the aircraft as intended. He could adjust the pitch for the desired g-level and then release the stick once the target attitude was reached. Pilot 2 mentioned aiming for the top of the reference square to avoid deviating beyond the margins with the dropback.
- **Flight Conditions:** In addition to the distinct dynamics already observed between conditions in the bare airframe, Pilot 2 also identified varying dynamics in the augmented aircraft. Specifically, he noted that FC1 exhibited more dropback compared to FC2 and FC3. Consequently, he found the aircraft to be more responsive in the latter conditions, necessitating fewer adjustments.

H. Discussion

The results were consistent with the hypotheses. The following paragraphs provide a detailed discussion of these findings.

1. Attitude

From the results, there is no doubt the attitude response of the augmented aircraft is as good as possible. The pilots described it as effortless and precise and clearly stated they preferred it. The consistent HQR of 1 is undeniable proof of this. It can be concluded that the Gibson dropback criterion in particular is very accurate in predicting an HQR of 1 for attitude control tasks. The pilots highly appreciate having little dropback in the response and this criterion is a perfect way to anticipate this situation. Additionally, the pilots also favored the attitude hold function provided by the RCAH. This resulted in less workload because the stick could just be released to maintain attitude instead of having to give continuous adjustment inputs. When testing lateral maneuvers, it may be necessary to add an additional attitude outer loop to strengthen the hold mode against potential pitch angle disturbances caused by these maneuvers. Finally, the pitch rate sensitivity criterion method for defining the sidestick dynamics was also validated. This method should ideally be combined with flight envelope protections since it is designed for good attitude response and does not take into account the structural limitations of the aircraft (like the stick force per g criterion). Integrating these three factors — Gibson dropback criterion, RCAH, and pitch rate sensitivity criterion - proved to be a powerful approach that ensures great handling qualities in the attitude control of passenger aircraft.

2. Flight Path

The results showed that Pilot 1 preferred the flight path response of the augmented aircraft, whereas Pilot 2 preferred the bare airframe. This aligns with the expectation that the two configurations would perform similarly, highlighting individual differences in control approaches among pilots. The CAP criterion effectively predicted Level 1 HQRs, but it alone cannot guarantee an HQR of 1. Therefore, to enhance the flight path response of the RCAH system, other handling quality criteria might have to be included in the controller design phase. Some criteria suggestions are the flight path response to attitude change [28], the flight path bandwidth [37], and the flight path time delay [29]. Another recommendation is to substitute the flight path tracking task for a landing with a longitudinal offset [30] as this may be a more realistic representation of actual flight conditions. This approach ensures that the task difficulty is appropriate

for the intended purpose of the aircraft. Overly challenging tasks can result in lower HQRs, which do not necessarily represent the true handling qualities of the aircraft but rather the excessive difficulty of the task itself. The disadvantage of this alternative task is that it requires more time to configure in the simulation, as it significantly differs from the other tasks. For instance, glideslope information must be incorporated, and the pilot may need to adjust the aircraft configuration during the task, such as deploying flaps or lowering the landing gear which adds a new degree of difficulty to the implementation. Lastly, it should be kept in mind that flight path control through attitude change might have insuperable performance limitations since the pilot is always indirectly controlling the flight path.

3. Changing Dynamics

As the speed and altitude increased in the bare airframe, pilots experienced more difficulties. The theoretical dropback increased from FC1 to FC3, anticipating progressively worsening responses. Hence, the difficulties found by the pilots were expected. In contrast, the augmented aircraft was designed to maintain a specific dynamic response. The results showed that the designed controller was able to ensure the differences between responses were negligible and not noticeable by pilots during the pitch tracking task. Only during pitch capture did Pilot 2 begin to notice some variations. If wanted, this situation can be straightforwardly adjusted by designing individual controllers for each flight condition and then using gain scheduling to integrate them. This process allows designers to select the desired response model based on the handling qualities and ensure consistency across different conditions. The flight path response differed between flight conditions in both configurations, and both pilots observed these changes. In the bare airframe, it was seen in Section III that the dynamics change across the trim envelope and so this was expected. In the augmented airframe, this variation was also expected since the flight path response was not being enforced by a reference model. Different responses between flight conditions are not inherently detrimental if good handling qualities are maintained and the changes are not abrupt.

4. Level of Agressiveness

In the tracking tasks, pilots were slightly more aggressive than they would be when prioritizing passenger comfort. Balancing realism with sufficient stress on the aircraft to identify deficiencies and test emergency scenarios is essential. The control approach recommended to the pilots aimed to achieve this balance. Now that the control design method has been validated, it is recommended to stress the aircraft with turbulence, disturbances, and/or uncertainties (such as extreme variation of aerodynamic coefficients or the position of the center of mass) rather than with challenging forcing functions and aggressiveness. This way, it is possible to ask the pilot to keep the passengers satisfied while stressing the aircraft at the same time, which is a more reasonable and less ambiguous request for the pilot.

VII. Conclusion

This article described a practical procedure for designing fixed-order control laws that integrate handling qualities and robust stability specifications directly into the optimization process for tuning controller parameters. Additionally, a multi-objective approach was also tested to obtain better trade-offs and less conflict between specifications. Initial analysis of the bare airframe of the PH-LAB Cessna Citation showed the attitude response had an excessively high dropback. After the implementation of the control law, pilots deemed the attitude response as having great handling qualities for considerably different flight conditions. This response was consistently preferred over that of the bare airframe. In the flight path response, the control law maintained the already existent level 1 handling qualities. Achieving such results with a single set of controller parameters proves that the control design method is able to produce remarkable robust performance, validating the anticipated benefits of the structured 2DoF $\mathcal{H}_\infty$ loop-shaping approach. These promising findings are expected to inspire further research, serving as a significant step toward the overarching goal of enhancing the safety of flight control systems.

References

[1] Weiser, C., Ossmann, D., and Looye, G., "Design and flight test of a linear parameter varying flight controller," *CEAS Aeronautical Journal*, Vol. 11, 2020, pp. 955–969.

[2] Slotine, J. J. E., and Li, W., *Applied nonlinear control*, Prentice Hall, 1991.

[3] Toscano, R., *Structured controllers for uncertain systems*, Springer, 2013.

[4] Apkarian, P., and Noll, D., "Nonsmooth H∞ synthesis," *IEEE Transactions on Automatic Control*, Vol. 51, 2006, pp. 71–86.

[5] Falcoz, A., Pittet, C., Bennani, S., Guignard, A., Bayart, C., and Frapard, B., "Systematic design methods of robust and structured controllers for satellites: Application to the refinement of Rosetta's orbit controller," *CEAS Space Journal*, Vol. 7, No. 3, 2015, pp. 319–334.

[6] Pittet, C., and Prieur, P., "Structured accelero-stellar estimator for MICROSCOPE drag-free mission," *Advances in Aerospace Guidance, Navigation and Control: Selected Papers of the Third CEAS Specialist Conference on Guidance, Navigation and Control held in Toulouse*, Springer, 2015, pp. 591–604.

[7] Marcos, A., and Sato, M., "Flight testing of a structured H-infinity controller: An EU-Japan collaborative experience," *2017 IEEE Conference on Control Technology and Applications (CCTA)*, IEEE, 2017, pp. 2132–2137.

[8] Apkarian, P., Gahinet, P., and Buhr, C., "Multi-model, multi-objective tuning of fixed-structure controllers," *2014 European Control Conference (ECC)*, IEEE, 2014, pp. 856–861.

[9] Limebeer, D. J., Kasenally, E. M., and Perkins, J. D., "On the design of robust two degree of freedom controllers," *Automatica*, Vol. 29, No. 1, 1993, pp. 157–168.

[10] McFarlane, D., and Glover, K., "A loop-shaping design procedure using H∞ synthesis," *IEEE transactions on automatic control*, Vol. 37, No. 6, 1992, pp. 759–769.

[11] Glover, K., Vinnicombe, G., and Papageorgiou, G., "Guaranteed multi-loop stability margins and the gap metric," *Proceedings of the 39th IEEE Conference on Decision and Control (Cat. No.00CH37187)*, Vol. 4, 2000, pp. 4084–4085 vol.4.

[12] Bates, D., and Postlethwaite, I., *Robust multivariable control of aerospace systems*, DUP Science, 2002.

[13] Grondman, F., Looye, G., Kuchar, R. O., Chu, Q. P., and Van Kampen, E.-J., "Design and flight testing of incremental nonlinear dynamic inversion-based control laws for a passenger aircraft," *2018 AIAA Guidance, Navigation, and Control Conference*, 2018, p. 0385.

[14] van't Veld, R., Van Kampen, E.-J., and Chu, Q. P., "Stability and robustness analysis and improvements for incremental nonlinear dynamic inversion control," *2018 AIAA Guidance, Navigation, and Control Conference*, 2018, p. 1127.

[15] Keijzer, T., Looye, G., Chu, Q. P., and Van Kampen, E.-J., "Design and flight testing of incremental backstepping based control laws with angular accelerometer feedback," *AIAA Scitech 2019 Forum*, 2019, p. 0129.

[16] Lee, J. H., and van Kampen, E.-J., "Online reinforcement learning for fixed-wing aircraft longitudinal control," *AIAA Scitech 2021 Forum*, 2021, p. 0392.

[17] Kaushal, J., "Evaluation and Comparison of Linear Quadratic Control Techniques," Master's thesis, Delft University of Technology, 2024.

[18] Boughari, Y., Botez, R. M., Theel, F., and Ghazi, G., "Optimal flight control on Cessna X aircraft using differential evolution," *International Association of Science and Technology for Development IASTED Modelling, Identification and Control (MIC 2014), Innsbruck, Austria*, 2014, pp. 189–198.

[19] Boughari, Y., Botez, R. M., Ghazi, G., and Theel, F., "Flight control clearance of the Cessna Citation X using evolutionary algorithms," *Proceedings of the Institution of Mechanical Engineers, Part G: Journal of Aerospace Engineering*, Vol. 231, No. 3, 2017, pp. 510–532.

[20] Berger, T., Tischler, M., and Hagerott, S. G., "Piloted simulation handling qualities assessment of a business jet fly-by-wire flight control system," *AIAA Atmospheric Flight Mechanics Conference*, 2015, p. 0019.

[21] Stroosma, O., Van Paassen, M., and Mulder, M., "Using the SIMONA research simulator for human-machine interaction research," *AIAA modeling and simulation technologies conference and exhibit*, 2003, p. 5525.

[22] Joosten, S., Stroosma, O., Vos, R., and Mulder, M., "Simulator Assessment of the Lateral-Directional Handling Qualities of the Flying-V," *AIAA SCITECH 2023 Forum*, 2023, p. 0906.

[23] Torelli, R., Stroosma, O., Vos, R., and Mulder, M., "Piloted Simulator Evaluation of Low-Speed Handling Qualities of the Flying-V," *AIAA SCITECH 2023 Forum*, 2023, p. 0907.

[24] Van der Linden, C., *DASMAT: Delft University Aircraft Simulation Model and Analysis Tool*, University of Technology, 1996.

[25] Van den Hoek, M., de Visser, C., and Pool, D., "Identification of a Cessna Citation II model based on flight test data," *Advances in Aerospace Guidance, Navigation and Control: Selected Papers of the Fourth CEAS Specialist Conference on Guidance, Navigation and Control Held in Warsaw, Poland, April 2017*, 2017, pp. 259–277.

[26] Skogestad, S., and Postlethwaite, I., *Multivariable feedback control: analysis and design*, John Wiley & Sons, 2005.

[27] Cooper, G. E., and Harper, R. P., *The use of pilot rating in the evaluation of aircraft handling qualities*, National Aeronautics and Space Administration, 1969.

[28] "MIL-STD-1797A," Tech. rep., US Department of Defence, 1990.

[29] Gibson, J., "Development of a Design Methodology for Handling Qualities Excellence in Fly-by-Wire Aircraft," Ph.D. thesis, Delft University of Technology, 1999.

[30] Castro, H. V., "Flying and handling qualities of a fly-by-wire blended-wing-body civil transport aircraft," Ph.D. thesis, Cranfield University, 2003.

[31] Smit, B., Pollack, T., and Van Kampen, E.-J., "Adaptive incremental nonlinear dynamic inversion flight control for consistent handling qualities," *AIAA SCITECH 2022 Forum*, 2022, p. 1394.

[32] "EASA.IM.A.207: Cessna 500, 550, S550, 560 and 560XL," Tech. rep., EASA, 2022.

[33] Stevens, B. L., Lewis, F. L., and Johnson, E. N., *Aircraft control and simulation: dynamics, controls design, and autonomous systems*, John Wiley & Sons, 2015.

[34] Chilali, M., and Gahinet, P., "H∞ design with pole placement constraints: an LMI approach," *IEEE Transactions on automatic control*, Vol. 41, No. 3, 1996, pp. 358–367.

[35] El-Sakkary, A., "The gap metric: Robustness of stabilization of feedback systems," *IEEE Transactions on Automatic Control*, Vol. 30, No. 3, 1985, pp. 240–247.

[36] Georgiou, T. T., and Smith, M. C., "Optimal robustness in the gap metric," *Proceedings of the 28th IEEE Conference on Decision and Control*, IEEE, 1989, pp. 2331–2336.

[37] Field, E. J., Rossitto, K. F., and Mitchell, D. G., "Landing approach flying qualities criteria for active control transport aircraft," *RTO AVT Symposium, Active Control Technology for Enhanced Performance Operational Capabilities of Military Aircraft, Land Vehicles and Sea Vehicles*, 2000, pp. 33–1.